Use of threshold electron and fluorescence coincidence techniques to probe the decay dynamics of the valence states of CF+4, SiF+4, SiCl+4, and GeCl+4

Smith, D. M.; Tuckett, R. P.; Yoxall, K. R.; Codling, K.; Hatherly, P. A.; Aarts, J. F. M.; Stankiewicz, M.

DOI:
10.1063/1.467873

Use of threshold electron and fluorescence coincidence techniques to probe the decay dynamics of the valence states of CF_4^+, SiF_4^+, $SiCl_4^+$, and $GeCl_4^+$

D. M. Smith, R. P. Tuckett, and K. R. Yoxall
School of Chemistry, University of Birmingham, Edgbaston, Birmingham B15 2TT, United Kingdom

K. Codling and P. A. Hatherly
J. J. Thomson Physical Laboratory, University of Reading, Whiteknights, Reading RG6 2AF, United Kingdom

J. F. M. Aarts
Department of Chemistry, Gorlaeus Laboratories, University of Leiden, 2300 RA Leiden, The Netherlands

M. Stankiewicz
Department of Physics, Jagellonian University, 30-059 Krakow, Poland

(Received 20 July 1994; accepted 13 September 1994)

Threshold photoelectron–photoion coincidence (TPEPICO), photoion–fluorescence coincidence (PIFCO), and threshold photoelectron–fluorescence coincidence (TPEFCO) spectroscopies have been used to measure, state selectively, the decay pathways of all the valence states of four gas-phase tetrahedral ion CF_4^+, SiF_4^+, $SiCl_4^+$, and $GeCl_4^+$ in the range 11–26 eV. Vacuum UV radiation from a synchrotron source dispersed by a 5 m normal-incidence McPherson monochromator ionizes the parent molecule, and electrons and ions are detected by threshold electron analysis and time-of-flight mass spectrometry, respectively. Undispersed fluorescence from the interaction region can also be detected, allowing the three different types of coincidence experiment to be performed. The optimum resolution of the monochromator is matched to that of the threshold analyzer, and this work improves on preliminary results using a 1 m Seya monochromator [Chem. Phys. **174**, 441 and 453 (1993)] where the resolution of the spectra was limited by that of the optical source. TPEPICO spectra are recorded continuously as a function of photon energy, allowing both threshold photoelectron spectra and yields of all the fragment ions to be obtained. Kinetic energy releases can also be measured at fixed photon energies with good time resolution. PIFCO and TPEFCO spectra are recorded at fixed photon energies. The former experiment can yield the fate of the lower electronic state of the parent ion to which fluorescence occurs. The latter experiment yields the lifetime of the fluorescing state; with sufficient resolution of the photoionizing radiation, the lifetime is specific to one vibrational level of the emitting electronic state. For CF_4^+ and SiF_4^+ work has concentrated on the third and fourth excited states, $\tilde{C}\ ^2T_2$ and $\tilde{D}\ ^2A_1$, of which only the $\tilde{C}$ state of SiF_4^+ does not decay radiatively. Vibrationally state-selected fluorescence quantum yields and lifetimes have been measured for four levels of the $\tilde{C}$ state of CF_4^+, and absolute values of radiative and nonradiative decay rates have been evaluated for these levels. Jahn–Teller distortion of the $\tilde{C}$ state of SiF_4^+ from T_d to C_{3v} geometry assists internal conversion of the $\tilde{C}\ ^2T_2$ state into high vibrational levels of the $\tilde{B}\ ^2E$ state, and is an efficient route for nonradiative decay. A non-Franck–Condon distribution of intensities is observed in the threshold photoelectron spectrum of the $\tilde{D}\ ^2A_1$ state of CF_4^+, due to autoionization from a high-lying Rydberg state of neutral CF_4. For the two chloride molecules, $SiCl_4$ and $GeCl_4$, fragmentation of the ground ($\tilde{X}$) and the first four excited states ($\tilde{A}$–$\tilde{D}$) of the parent ion have been studied at slightly lower resolution. For $SiCl_4^+$ an important result is confirmation of the stability of its electronic ground state with respect to dissociation to $SiCl_3^+ + Cl$. By contrast, a substantial part of the Franck–Condon zone of the ground state of $GeCl_4^+$ is energetically unstable with respect to $GeCl_3^+ + Cl$. Radiative decay from the $\tilde{C}\ ^2T_2$ state of both ions is an important process. The decay dynamics of all the valence states of this family of tetrahedral ions are reviewed. Dynamical, rather than statistical, processes generally dominate, and reasons for these surprising phenomena are discussed. © *1994 American Institute of Physics.*

I. INTRODUCTION

It is now well-established that coincidence experiments offer a powerful technique to determine the decay dynamics of selected vibronic states of positively charged molecular ions. For singly ionization events, the most commonly used is the photoelectron–photoion coincidence (PEPICO) technique in which energy-analyzed photoelectrons are detected in delayed coincidence with ions which have been mass selected in a time-of-flight (TOF) mass spectrometer. For the specific case in which the electrons have zero energy, this technique is called the threshold photoelectron–photoion co-

incidence (TPEPICO) experiment, and is the form that is usually used if the photoionization source is tunable in energy. Less well known but just as informative are two coincidence techniques that can be used if the electronic state of the ion under study decays radiatively by photon emission. These are the photoion–fluorescence coincidence (PIFCO) and photoelectron–fluorescence coincidence (PEFCO) techniques. If a threshold, zero energy electron is detected, the latter technique has the acronym TPEFCO.

The information that can be obtained from these three different coincidence experiments is varied. PEPICO/TPEPICO spectroscopy allows the fragmentation channels of both ground and excited electronic states of ions to be studied. If the electron analyzer and photon beam have sufficient resolution, these measurements can usually be made with vibrational resolution in the parent molecular ion. The fragment ion channels that are observed and the kinetic energy (KE) released into these channels are important guides to statistical or dynamical behavior in the ion. PIFCO spectroscopy can be used to determine whether an excited state of a molecular ion decays by a radiative process. If coincidences are observed it is possible to measure the fluorescence quantum yield, $\Phi_F[=k_r/(k_r+k_{nr})]$, and lifetime, $\tau\,[=(k_r+k_{nr})^{-1}]$, where k_r and k_{nr} are radiative and nonradiative decay rates of the excited electronic state of the molecular ion, but these quantities are averaged over the Franck–Condon populations of the vibrational levels of the fluorescing state. By observing which ion is detected in coincidence with the photon, the fate of the lower electronic state to which fluorescence occurs can be determined. The PEFCO/TPEFCO technique can also be used to measure Φ_F and τ, but now the resolution is determined by that of the photoionizing beam and the electron analyzer. In this way vibrational state selectivity can often be obtained. Changes of $(\Phi_F)_v$ and τ_v with vibrational level (v) are especially revealing because they can usually be attributed to a change in k_{nr}, i.e., the onset of a competing nonradiative channel. This experiment is usually more demanding than the PIFCO experiment because of the lower signal levels.

In a recent paper[1] we described an apparatus for performing TPEPICO experiments which can be attached to a vacuum ultraviolet (VUV) beam line at the UK synchrotron source at Daresbury, and results obtained for the fragmentation of the valence states of CF_4^+, SF_6^+, CCl_4^+, and $SiCl_4^+$ have subsequently been reported.[2,3] Although the apparatus is optimized for this type of coincidence experiment, the addition of collection optics and a photomultiplier tube for undispersed fluorescence detection means that PIFCO and TPEFCO experiments can also be performed, and some preliminary results were reported for radiative decay of the $\tilde{C}\,^2T_2$ excited valence electronic state of CF_4^+.[4] All these results were obtained using a 1 m Seya monochromator for production of the tunable photon beam. This monochromator, whose energy range is 10–35 eV, has a best resolution in the scanning mode of 0.06 nm, corresponding to 0.019 eV at 20 eV. This resolution is a factor of 5 inferior to that predicted for the threshold electron analyzer,[1] and therefore the resolution of all the spectra are limited by the monochromator and not by the threshold electron analyzer. Furthermore, all three types of coincidence experiment are, in practice, flux limited, and the relative poor flux of the Seya monochromator ($\sim 10^{10}$ photons per second per 0.1% bandwidth per 100 mA beam current) means that accumulation times are often very long. In this paper, we report our first results obtained using the higher-resolution 5 m McPherson monochromator (range 10–30 eV) at the Daresbury source. This monochromator has both better resolution (down to 0.01 nm in the scanning mode) and flux ($\sim 5\times 10^{11}$ photons per second per 0.1% bandwidth per 100 mA beam current), so not only is the resolution of the monochromator better matched to that of the threshold electron analyzer but also data accumulation times are substantially reduced. We report results for four tetrahalide ions (CF_4^+, SiF_4^+, $SiCl_4^+$, and $GeCl_4^+$) using the three coincidence experiments described above. The results for CF_4^+ and $SiCl_4^+$ complement and extend those obtained with the lower-resolution Seya monochromator.[2,3] The results for SiF_4^+ and $GeCl_4^+$ are new since these ions have not been studied before by state-selected coincidence techniques which involve energy analysis of the photoelectrons; our early electron–ion coincidence experiments on these two ions using tunable synchrotron radiation[5] employed no energy analyzer for the photoelectrons, so the initial state of the parent ion could not be uniquely determined.

II. EXPERIMENT

The coincidence apparatus has been described in detail elsewhere.[1–3] VUV radiation from a 5 m McPherson normal-incidence monochromator attached to the Daresbury synchrotron source is admitted to the interaction region through a capillary. The grating is blazed at 55 nm, and has a range of ~35–100 nm with second-order effects contributing ~20% for wavelengths greater than 80 nm. The photon flux is monitored through a sodium salicylate coated window by a photomultiplier tube, allowing flux normalization of the data. The threshold electron analyzer incorporates a cylindrical electrostatic lens designed with large chromatic aberrations, followed by a 127° post-analyzer which rejects the energetic electrons on axis. Even with an extraction field as large as 20 V cm^{-1}, simulations predict that the analyzer has both high collection efficiency (100% for zero-energy electrons) and high resolution (~3.5 meV half-width). Experiments on photoionization of argon (Sec. IV A) have now confirmed that these predictions are essentially true. The ion detector consists of a two-stage acceleration region and a field-free region configured to satisfy the space focusing condition,[6] allowing measurement of the KE release from a dissociative ionization process while still retaining a high collection efficiency. The electron and ion signals are detected by a channeltron electron multiplier (Phillips X818BL) and a pair of microchannel plates (Galileo MCP-40/32), respectively. Fluorescence from the interaction region orthogonal to the direction of the electron and ion flight paths is collected by an $f/1$ biconvex lens of focal length 50 mm and detected by a photon-counting photomultiplier tube cooled to 253 K. For the CF_4^+ experiments (Sec. IV B) a Mullard 2020QB tube (wavelength range 200–550 nm) was used, for the SiF_4^+, $SiCl_4^+$, and $GeCl_4^+$ experiments (Secs. IV C–IV E) a Mullard

2254QB red-sensitive tube (wavelength range 200–750 nm) was used. An $f/1$ concave mirror of focal length 75 mm placed behind the interaction region serves to enhance the collection efficiency. The raw pulses from the electron, ion, and photon detectors are passed to discriminator and pulse-shaping circuits (based on the LeCroy HVL 100 discriminator for the electron and ion signals), and any two of them are fed into a time-to-digital converter (TDC, LeCroy 4208) configured in the "multihit" mode. One provides the start pulses, the other the stop pulses, hence the two signals from the same ionization event are detected in delayed coincidence. Interchange between the different forms of coincidence experiment is straightforward. The scanning of the monochromator and the collection of the coincidence data are controlled by two IBM personal computers (PCs) which interact through CAMAC-based electronics.

This apparatus is very versatile, and can perform the following experiments. First, a threshold photoelectron spectrum (TPES) of the sample gas can be recorded as a function of photon energy. By this method, the monochromator can be calibrated over its complete range by recording the TPES of O_2 into low vibrational levels of the $X\ ^2\Pi_g$ ground state of O_2^+ around 12 eV, into the $B\ ^2\Sigma_g^-$ state around 20 eV and into the $c\ ^4\Sigma_u^-$ state around 25 eV. We use the values from Baltzer[7] for these energies. Peak positions can generally be measured to an accuracy of at least one-third of the monochromator resolution. Second, all three kinds of coincidence experiment (TPEPICO, PIFCO, and TPEFCO) can be recorded at a fixed photon energy. In a TPEPICO spectrum of this kind, the fragments ions often have substantial translational KE release and, to obtain the kinetic energy release distribution (KERD),[8] TOF data are accumulated at as high a time resolution of the TDC as the signal level will permit. In PIFCO and TPEFCO spectra of this kind, coincidence count rates are much lower, primarily because the apparatus is not optimized for experiments with fluorescence detection, and time resolution is then sacrificed in order to obtain a spectrum in a reasonable period of time. Thus, we use the PIFCO experiment solely to determine whether an excited state of a molecular ion fluoresces, and if so which ion is in coincidence with the photon; this determines the fate of the lower electronic state to which fluorescence occurs. In a TPEFCO spectrum the electron signal provides the start, the fluorescence signal the stop pulses. The latter are subjected to an arbitrary but constant delay of ~900 ns in order to separate the almost simultaneous start and stop pulses at the TDC. This delay results in a time offset in TPEFCO spectra. The time resolution of the experiment is limited by that of the TDC, in our case 1 ns. Third, a TPEPICO spectrum can be recorded continuously as a function of photon energy. Usually all the ions produced in the TPEPICO spectrum are recorded in this energy-scanning mode, and the resolution of the TDC is correspondingly degraded. Data accumulate as a three-dimensional histogram of photon energy versus ion TOF versus coincidences, the last variable being displayed in color on the data-collection PC.[9] Data are displayed by taking cross-sectional cuts through the histogram, the most useful being the variation of a fragment ion yield with photon energy. The total electron count is also recorded by the PC that controls the scanning of the monochromator, so a threshold photoelectron spectrum can be displayed simultaneously with the yields of the fragment ions. Although it should be possible, we do not run the PIFCO and TPEFCO experiments in this energy-scanning mode. It should be noted that all these experiments run in the "multibunch" quasi-cw mode of the synchrotron source, and pulsed extraction is not used for either electron or ion detection.

CF_4 and SiF_4 gases (Air Products Ltd.) were used without further purification. $SiCl_4$ and $GeCl_4$ liquids (Aldrich Co.) were subject to several freeze–pump–thaw cycles before admission to the apparatus. The base pressure of the apparatus is typically 5×10^{-8} Torr, while the background pressure during an experiment is between 3×10^{-5} and 1×10^{-4} Torr.

III. THE ENERGETICS AND DISSOCIATION CHANNELS OF MX_4^+(M=C,Si,Ge: X=F, Cl)

The electron configuration of the five highest-occupied outervalence molecular orbitals of the molecules under study is $\cdots(2a_1)^2(2t_2)^6(1e)^4(3t_2)^6(1t_1)^6$, where the numbering scheme does not include the core orbitals. Adiabatic ionization potentials (IPs) are given in Table I, the data being taken from He I or He II photoelectron spectroscopy.[10–13] Also shown are the energies of the neutral and ionic dissociation channels of $MX_4^{(+)}$. For CF_4 and $SiCl_4$ the neutral dissociation energies are calculated from heats of formation at 0 K given in the JANAF tables,[14] for SiF_4 we use values recommended very recently from studies of charge-transfer reactions of atomic ions with SiF_4,[15] and for $GeCl_4$ we use data derived from two relatively old sources.[16] In all cases the uncertainties in these energies are very small. The energies of the ionic dissociation channels are calculated using what we believe is the best value for the IPs of the neutral fragments MX_n ($n=1$–3), the references being given as a footnote to the table. Two major points about this data should be noted. First, the ground states of the parent ion lie at different energies with respect to the lowest dissociation channels to $MX_3^+ + X$. Thus the ground state of CF_4^+ as accessed by Franck–Condon ionization from neutral CF_4 lies in a repulsive region at least 1 eV above the dissociation energy of $CF_3^+ + F$, whereas this state of SiF_4^+ lies at approximately the same energy as that of $SiF_3^+ + F$. The ground state of $SiCl_4^+$ is stable with respect to dissociation to $SiCl_3^+ + Cl$ by ~1 eV, whereas that of $GeCl_4^+$ is only stable by 0.4 eV. (The $GeCl_4^+/GeCl_3^+$ result assumes an old "indirect" value for the IP of $GeCl_3$ of 9.34 eV.[16] This value is calculated from an appearance potential of $GeCl_3^+$ from $GeCl_4$ by electron-impact mass spectrometry, and is an upper limit. It is likely, therefore, that the dissociation energy of $GeCl_3^+ + Cl$ lies below 12.12 eV, with most parts of the $GeCl_4^+$ ground state potential being unstable.) Second, vibrational structure is resolved in the photoelectron spectra of some of the higher valence ionic bands, namely the $\tilde{C}\ ^2T_2$ and $\tilde{D}\ ^2A_1$ states, and where this is the case adiabatic IPs are quoted to two decimal places. These are the states from which radiative decay can be observed. Such emission is surprising and is one manifestation of nonstatistical behavior in these ions because, for five-atom polyatomics composed of heavy atoms, nonradia-

TABLE I. Energetics of dissociation channels of $CF_4^{(+)}$, $SiF_4^{(+)}$, $SiCl_4^{(+)}$, and $GeCl_4^{(+)}$.

Neutral/parent ion		Dissociation channel	Dissociation energy/eV[a]	Adiabatic IP/eV[b]
CF_4^+	$\tilde{D}\ ^2A_1$			25.07[c]
		$CF_2+F_2^+$	23.4	
		CF_3+F^+	23.0	
		CF^++F+F_2	22.1	
	$\tilde{C}\ ^2T_2$			21.66[c]
		CF_2^++F+F	20.9	
		$CF_2^++F_2$	19.3	
	$\tilde{B}\ ^2E$			18.3
	$\tilde{A}\ ^2T_2$			17.1
	$\tilde{X}\ ^2T_1$			15.3[d]
		CF_3^++F	14.2	
		$CF+F+F_2$	13.0	
		CF_2+F_2	7.7	
		CF_3+F	5.6	
CF_4	$\tilde{X}\ ^1A_1$			0
		SiF^++F+F_2	24.1	
SiF_4^+	$\tilde{D}\ ^2A_1$			21.55[c]
		$SiF_2^++F_2$	20.9	
	$\tilde{C}\ ^2T_2$			19.30[c]
	$\tilde{B}\ ^2E$			18.0
	$\tilde{A}\ ^2T_2$			17.3
		$SiF+F+F_2$	17.0	
		SiF_3^++F	16.2	
	$\tilde{X}\ ^2T_1$			16.1[e]
		SiF_2+F_2	10.1	
		SiF_3+F	7.2	
SiF_4	$\tilde{X}\ ^1A_1$			0
$SiCl_4^+$	$\tilde{D}\ ^2A_1$			18.11[c]
		$SiCl_3+Cl^+$	17.8	
		$SiCl_2^++Cl+Cl$	17.7	
		$SiCl^++Cl+Cl_2$	16.8	
		$SiCl_2+Cl_2^+$	16.6	
		$SiCl_2^++Cl_2$	15.2	
	$\tilde{C}\ ^2T_2$			15.0[c]
	$\tilde{B}\ ^2E$			13.2[c]
	$\tilde{A}\ ^2T_2$			12.6[c]
		$SiCl_3^++Cl$	12.7	
	$X\ ^2T_1$			11.8[c]
		$SiCl+Cl+Cl_2$	10.0	
		$SiCl_2+Cl_2$	5.1	
		$SiCl_3+Cl$	4.8	
$SiCl_4$	$\tilde{X}\ ^1A_1$			0
$GeCl_4^+$	$\tilde{D}\ ^2A_1$			18.2
		$GeCl_2^++Cl+Cl$	16.0	
		$GeCl_3+Cl^+$	15.8	
		$GeCl^++Cl+Cl_2$	15.1	
		$GeCl_2+Cl_2^+$	14.8	
	$\tilde{C}\ ^2T_2$			14.6
		$GeCl_2^++Cl_2$	13.5	
	$\tilde{B}\ ^2E$			12.8[c]
	$\tilde{A}\ ^2T_2$			12.4[c]
		$GeCl_3^++Cl$	12.1[c]	
	$\tilde{X}\ ^2T_1$			11.7[c]
		$GeCl+Cl+Cl_2$	7.9	
		$GeCl_2+Cl_2$	3.3	
		$GeCl_3+Cl$	2.8	
$GeCl_4$	$\tilde{X}\ ^1A_1$			0

[a]Calculated using adiabatic ionization potentials of CF_3 of 8.6 eV (Ref. 17), CF_2 of 11.6 eV (Ref. 18), CF of 9.1 eV (Ref. 19), SiF_3 of 9.0 eV (Ref. 15), SiF_2 of 10.8 eV (Ref. 20), SiF of 7.3 eV (Ref. 21), $SiCl_3$ of 7.9 eV (Ref. 22), $SiCl_2$ of 10.1 eV (Ref. 23), SiCl of 6.8 eV (Ref. 21), $GeCl_2$ of 10.2 eV (Ref. 24), GeCl of 7.2 eV (Ref. 25), F of 17.4 eV and Cl of 13.0 eV (Ref. 14), F_2 of 15.7 eV and Cl_2 of 11.5 eV (Ref. 26).

[b]Unless otherwise stated, data for CF_4 from Ref. 10, for SiF_4 from Refs. 11 and 12, and for $SiCl_4$ and $GeCl_4$ from Ref. 13.

[c]This work.

[d]Difficult to measure because of the very small Franck–Condon factor at threshold.

[e]As footnote d. Kickel *et al.* (Ref. 27) quote a much lower value of 15.29 ±0.08 eV.

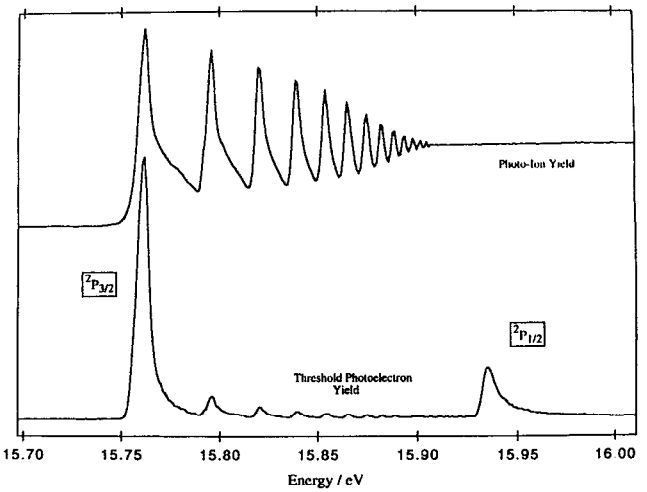

FIG. 1. Photoion yield and threshold photoelectron yield for $(3p)^{-1}$ photoionization of argon between 15.7 and 16.0 eV. The threshold electron signal is multiplied by a factor of 40. The photon resolution is 0.025 nm or ~5 meV.

tive processes (e.g., internal conversion, predissociation, or direct dissociation to lower-lying fragment ions) would be expected to dominate. These points summarize one of the general and surprising features of this family of singly charged group IV tetrahalide ions, that the ground state of many of the ions are unstable with respect to dissociation but some excited valence states are bound and have correspondingly longer lifetimes. The major consequence of this feature is that nonstatistical processes are a frequent occurrence.[9]

IV. RESULTS AND DISCUSSION

A. Argon

Figure 1 shows the threshold photoelectron and total photoion yield of argon as a function of photon energy from 15.7 to 16.0 eV for photoionization into the two spin–orbit states of Ar^+. The monochromator resolution has a full width at half-maximum of 0.025 nm, corresponding to 5 meV at this photon energy. The energies of the $Ar^+\ ^2P_{3/2}$ and $^2P_{1/2}$ thresholds are well established at 15.759 and 15.937 eV,[28] and for infinitely high resolution in both the photon source and the threshold analyzer the relative intensities of these two peaks should show a statistical ratio of 2:1. In practice the ratio is greater than this, ~5.5:1. The enhanced intensity in the $^2P_{3/2}$ peak arises because of the presence of high-lying neutral Rydberg states of argon that converge to the $Ar^+\ ^2P_{1/2}$ threshold. These states have greater energy than that of $Ar^+\ ^2P_{3/2}$ and decay by autoionization to this state, resulting in the production of energetic electrons and Ar^+ ions. The ions manifest themselves as resolved structure in the photoion yield,[29] the electrons as extra contributions to the threshold electron signal caused by direct ionization. The detection or suppression of these energetic electrons can be regarded as a stringent test of the resolution of the threshold analyzer. Thus the $11s,9d$ Rydberg states of Ar at 15.763 eV contribute by autoionization an electron with kinetic energy

of 4 meV, the $12s,10d$ states at 15.796 eV an electron with energy of 37 meV, etc. Since the electron analyzer is predicted to have a half-width at half-maximum (HWHM) of 3.5 meV,[1] the electron peak due to $Ar^+ {}^2P_{3/2}$ will have an enhanced intensity due to a major contribution from the autoionizing $11s,9d$ Rydberg state. This is indeed observed. Although the weak features in the threshold electron signal with peaks at energies of 15.796, 15.820, 15.839 eV, etc., show that the analyzer is not rejecting *totally* the energetic electrons, their suppression by the threshold analyzer is highly satisfactory. The $Ar^+ {}^2P_{1/2}$ threshold electron peak is not distorted by autoionizing states; it only arises from direct photoionization of argon. Therefore, the width of this peak is usually taken to be the most accurate measure of the resolution of a threshold electron analyzer. The HWHM on the high-energy side of this peak is measured to be 6 ± 1 meV. This width has contributions from both the photon beam and the threshold analyzer. If we assume these widths are Gaussian, then we can calculate the HWHM of the analyzer to be 4 meV. This value is in excellent agreement with that obtained by Monte Carlo simulation of a large number of electron trajectories.[1]

Ions are produced along the length of the photon beam in the interaction region (40 mm long $\times1$ mm $\times1$ mm), and are collected with 100% efficiency by the TOF mass spectrometer from a similar volume. However, our simulations predict that for 100% collection of threshold electrons the volume is only 10 mm $\times1$ mm $\times0.2$ mm (along the analyzer axis), corresponding to the center of the interaction region, and this value decreases rapidly for a larger interaction volume. The absolute collection efficiency of the threshold analyzer is therefore not easy to measure, but at the $^2P_{1/2}$ peak the ratio of the threshold electron signal to that of the Ar^+ yield is ~1:70. Given that the TOF mass spectrometer collects ions from an interaction volume which is 20 times greater for ions than for electrons, and assuming the detection efficiencies of the ion and electron detectors are similar, we estimate a collection efficiency for threshold electrons of 30% which is highly satisfactory.

B. Carbon tetrafluoride

Using the Seya monochromator, we have made two previous studies of the fragmentation of the five outervalence states of $CF_4^+(\tilde{X},\tilde{A},\tilde{B},\tilde{C},\tilde{D})$. First,[5] electron–ion coincidence spectra were recorded as a function of photon energy over the range 15–27 eV. In these experiments, there was no energy analysis of the photoelectrons and all electrons with energies from zero to 8 eV were collected with high efficiency. Therefore in no experiment was the internal energy of the CF_4^+ parent ion uniquely defined. CF_3^+ and CF_2^+ were the only two ions observed and their ion yield curves and thresholds for production were obtained. However, due to the lack of electron energy analysis the data for the kinetic energy released into these fragment ions at a particular photon energy were only of limited value, and it was not possible to say whether the fragmentation channels observed at each of the five electronic states of CF_4^+ were unique. Second,[2] TPEPICO spectra were recorded over the same range of photon energies using the apparatus described in this paper, now

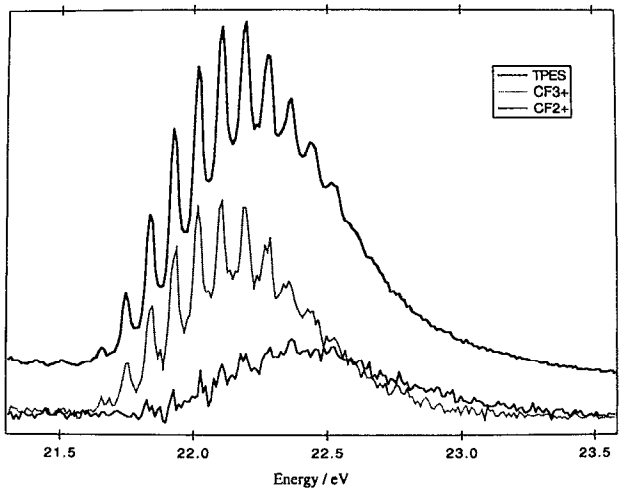

FIG. 2. Threshold photoelectron spectrum and coincidence yields of CF_2^+ and CF_3^+ from CF_4 between 21.4 and 23.5 eV. The photon resolution is 0.05 nm or ~0.02 eV.

with the internal energy of the CF_4^+ parent ion determined by that of the photon beam since the electron analyzer only collects zero-energy electrons. KERDs were measured at the Franck–Condon maximum of the five outervalence states of CF_4^+, and the average translational KE released into the fragment ions was determined. The information from the "energy-scanning" experiments, however, was limited by the relatively poor resolution of the photon beam, and due to the low photon flux accumulation times were very long.

In this study with the 5 m McPherson monochromator, we have not repeated the KERD measurements since they do not need high photon resolution. Instead we have concentrated our effort to study in detail fragmentation of the $\tilde{C}\ {}^2T_2$ and $\tilde{D}\ {}^2A_1$ states of CF_4^+ since these states exhibit vibrational resolution in their photoelectron spectra, decay radiatively by photon emission, and hence are most amenable to high-resolution study. The $\tilde{X}\ {}^2T_1$, $\tilde{A}\ {}^2T_2$, and $\tilde{B}\ {}^2E$ states of CF_4^+ lie below the energy of the He I resonance line (21.2 eV), and fragmentation of these states has been studied in some detail by us and others.[2,30–32] The $\tilde{X}$ and $\tilde{A}$ states show no vibrational structure in their photoelectron bands, the Franck–Condon accessible regions are repulsive in character, and assisted by Jahn–Teller distortion these states fragment on a subpicosecond time scale to $CF_3^+ + F$ with a large fraction of the available energy being deposited nonstatistically into relative translational motion of the two fragments. The $\tilde{B}$ band shows a partially resolved progression in ν_1 (810 cm^{-1}) and possibly ν_2(400 cm^{-1}), the latter again arising from Jahn–Teller distortion of this state from T_d symmetry. This state almost certainly undergoes rapid internal conversion into the $\tilde{A}$ state before fragmenting from the repulsive surface.[31] The $\tilde{C}$ and $\tilde{D}$ states of CF_4^+ have very recently been studied by threshold photoelectron spectroscopy[33] at slightly higher resolution than the work presented in this paper, but the state-selected fragmentation of these states using coincidence techniques has not been reported.

Figure 2 shows the TPEPICO spectrum of the $\tilde{C}\ {}^2T_2$

TABLE II. Positions of threshold photoelectron peaks in vibrationally resolved bands of CF_4^+ and SiF_4^+.[a]

CF_4^+			SiF_4^+			
ν_1	$\tilde{C}\ ^2T_2$	$\tilde{D}\ ^2A_1$	ν_1	ν_4	$\tilde{C}\ ^2T_2$	$\tilde{D}\ ^2A_1$[b]
0	21.656	25.074	0	0	19.302	21.554
1	21.746	25.170	0	1	19.354	
2	21.836	25.258	1	0	19.386	21.646
3	21.926	25.350	1	1	19.434	
4	22.016	25.438	2	0	19.474	
5	22.106	25.534	2	1	19.520	
6	22.196	25.622	3	0	19.564	
7	22.281		4	0	19.644	
8	22.361					
9	22.441					
10	22.516					

[a]Peak positions ±0.005 eV at 19 eV, ±0.006 eV at 21 eV, and ±0.008 eV at 25 eV, corresponding to one third of the resolution of the photoionization source.
[b]Weak shoulders at 21.586 and 21.700 eV assigned to $\nu_2=1$ and $\nu_3=1$, respectively.

state of CF_4^+ recorded in the energy-scanning mode at a photon resolution of 0.05 nm, corresponding to an energy resolution of ~0.02 eV. As noted above and in our previous work,[2] CF_3^+ and CF_2^+ are the fragment ions observed, and their yields are displayed in Fig. 2 together with the threshold photoelectron signal which is also recorded in these energy-scanning coincidence spectra. The long vibrational progression in the photoelectron spectrum is the ν_1 vibration, the energies of the bands are given in Table II, and we determine an adiabatic ionization potential for this state of 21.656±0.006 eV. This value is in excellent agreement with that determined from our earlier work using the Seya monochromator (21.67±0.03 eV),[2] but is slightly lower than that of Yencha *et al.* (21.677±0.004 eV).[33] The average vibrational spacing of 0.090±0.005 eV or 726±40 cm^{-1} is in excellent accord with that determined from a higher-resolution optical study of the $\tilde{D}-\tilde{C}$ electronic transition in CF_4^+ of 729±1 cm^{-1}.[34] At our resolution of 0.02 eV we see no evidence for other vibrational bands contributing to the structure of the photoelectron band, and we conclude that any Jahn–Teller distortion of this orbitally degenerate T_2 electronic state from tetrahedral symmetry is minimal. Structure in the ν_1 vibration is lost for $\nu_1>10$, suggesting that higher vibrational levels dissociate or predissociate at a rate greater than $\sim 10^{13}$ s^{-1}. The CF_3^+ yield matches the threshold photoelectron signal, with vibrational structure in ν_1 being observed for the first time in the ion yield. Since the yield has exactly the same shape and structure as the Franck–Condon envelope of the CF_4^+ $\tilde{C}$ state, as before[2] we believe that production of CF_3^+ arises indirectly from radiative decay of the $CF_4^+\tilde{C}$ state to the repulsive $\tilde{X}$ and $\tilde{A}$ states which dissociate directly to CF_3^++F. Unlike CF_3^+, the CF_2^+ ion arises from a competing, dissociative process of the $\tilde{C}$ state. It seems very likely that this process is nonradiative, because the $\tilde{X}$, $\tilde{A}$, and $\tilde{B}$ states of CF_4^+ (to which $\tilde{C}$-state fluorescence might occur) all lie *below* the lowest thermodynamic energy of CF_2^+ (Table I). The yield of CF_2^+ shows a gradual rise with a threshold at 21.85±0.05 eV, corresponding to the energy of $\nu_1=2$, a maximum ~0.3 eV to higher energy than that of the CF_3^+ ion, and partially resolved vibrational structure in the ν_1 band. We believe that the CF_2^+ signal may arise by a process of direct dissociation, probably involving the formation of a tightly constrained transition state at a barrier along the dissociation coordinate. By analogy with calculations on the $\tilde{A}\ ^1T_2$ lowest Rydberg state of CH_4,[35] it is possible that the $\tilde{C}\ ^2T_2$ state of CF_4^+ correlates adiabatically to the ground states of $CF_2^+(\tilde{X}\ ^2A_1)$ and $F_2(^1\Sigma_g^+)$. Excited states of CF_2^+ cannot be formed on energetic grounds.[18] Assuming the CF_3^+ signal arises solely from the radiative decay process described above, then at any photon energy the ratio of the CF_3^+ yield to that of CF_2^+ gives the ratio of $(\Phi_F)_v$ to $(1-(\Phi_F)_v$. Thus we obtain $(\Phi_F)_v=1$, 1, 0.90, 0.91, 0.87, 0.82, 0.77, 0.72, 0.63, 0.61, and 0.53 for $v_1=0-10$, respectively. The integrated area of the CF_3^+ signal to the CF_2^+ signal yields a vibrationally averaged value for the fluorescence quantum yield of the $CF_4^+\tilde{C}$ state, $(\Phi_F)_{\text{average}}=0.67\pm0.05$.

In our earlier work[4] a PIFCO spectrum was recorded at the Franck–Condon maximum of the $CF_4^+\tilde{C}$ state. Coincidences were only observed with ions whose time of flight corresponds to that of CF_3^+. Thus fluorescence from the $CF_4^+\tilde{C}$ state occurs to lower-lying states ($\tilde{A}\ ^2T_2$ and $\tilde{X}\ ^2T_1$) which dissociate promptly to CF_3^+. With sufficient time resolution it is possible to record the decay of the coincidence signal with time and obtain the vibrationally averaged lifetime of this state. This experiment was not performed on the Seya monochromator due to the weakness of the photon flux, and it has not been attempted on the McPherson because it is more informative to measure vibrationally state-selected lifetimes (τ_v) by the TPEFCO technique. Thus TPEFCO coincidence spectra were recorded at four different photon energies within the $CF_4^+\tilde{C}$ state Franck–Condon envelope, namely 21.84, 22.02, 22.20, and 22.36 eV corresponding to $\nu_1=2$, 4, 6, and 8, respectively. The optical resolution was 0.02 eV, no filter was used with the photomultiplier tube, and the highest time resolution of the time-to-digital converter (1 ns) was used. The results are shown in Fig. 3. The lifetimes of these four levels, τ_v, decrease monotonically from 9.0 to 7.9 ns as v_1 increases from 2 to 8. In our preliminary TPEFCO experiments[4] with the Seya monochromator where complete vibrational resolution was not possible, scarcely any change

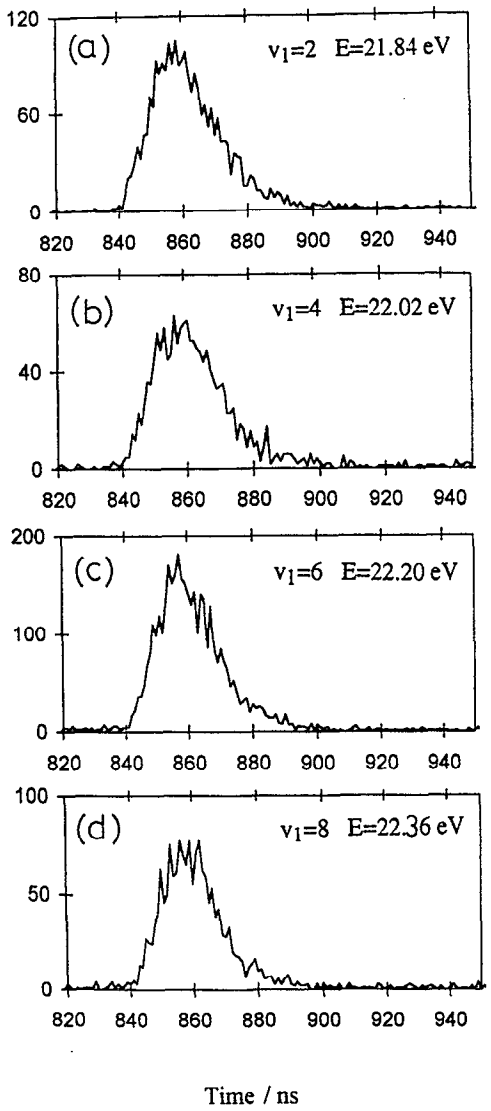

FIG. 3. TPEFCO spectra of the fluorescence from the $\tilde{C}\ ^2T_2$ state of CF_4^+ at excitation energies of (a) 21.84, (b) 22.02, (c) 22.20, and (d) 22.36 eV, corresponding to $v_1=2$, 4, 6, and 8, respectively. The photon resolution is 0.05 nm (~0.02 eV), the time resolution is 1 ns per channel, and the accumulation time of each spectrum is ~5 h.

in τ_v was observed over the range 21.9–22.8 eV. The surprise is not that the lifetime decreases as v_1 increases, but that the change is so small. The conclusions are described in full in our earlier publication. Briefly, k_r and k_{nr} are related to the observables $(\Phi_F)_v$ and τ_v by $k_r=(\Phi_F)_v/\tau_v$ and $k_{nr}=[1-(\Phi_F)_v]/\tau_v$, where $\tau_v=(k_r+k_{nr})^{-1}$. The TPEPICO data (Fig. 2) show clearly that $(\Phi_F)_v$ decreases as photon energy within the $CF_4^+\tilde{C}$ state (or v_1) increases. Hence for τ_v to vary so little with v_1, as v_1 increases k_r must decrease at approximately the same rate as k_{nr} increases to maintain (k_r+k_{nr}) approximately constant. The values obtained for k_r and k_{nr} for different values of v_1 are shown in Table III. The small values of k_{nr} must arise through slow intramolecular vibrational redistribution within the $CF_4^+\tilde{C}$ state. Photoionization only populates the ν_1 (a_1) manifold, whereas dissociation to $CF_2^+ + F_2$ must involve channeling the energy into the $\nu_2(e)$ vibrational mode. This process is relatively slow $(\sim 10^7-10^8\ s^{-1})$, allowing fluorescence to be an important competing decay pathway. The nonradiative process is presumably hindered by the high symmetry of the $\tilde{C}$ state and the corresponding low density of vibrational levels. However, k_{nr} increases for higher values of ν_1 (Table III) due to an increase in the density of vibrational levels as the barrier to dissociation is approached. This interpretation is substantiated by a recent analysis of Doppler-limited optical emission spectra of different vibronic bands of the $\tilde{D}(v_1'=0)-\tilde{C}(v_1'')$ transition in CF_4^+.[36] Perturbations become increasingly apparent in the rotational structure of the $\tilde{C}$ state as v_1'' increases, becoming marked for $v_1'' \geq 2$ as nonradiative processes become more important.

Figure 4 shows the TPEPICO spectrum of the $\tilde{D}\ ^2A_1$ state of CF_4^+ recorded in the energy-scanning mode at a photon resolution of 0.05 nm which now corresponds to an energy resolution of ~0.025 eV. Again, CF_3^+ and CF_2^+ are the fragment ions observed, and as in Fig. 2 we display their yields and the threshold photoelectron spectrum. The TPE spectrum shows a long progression in ν_1 extending up to $\nu_1=5$ or 6, peak positions are given in Table II, we obtain a value for ν_1 of 0.093±0.007 eV or 750±56 cm^{-1}, and this compares with a value of 800±1 cm^{-1} obtained from the high-resolution $\tilde{D}-\tilde{C}$ optical study.[34] This band shows a very

TABLE III. Fluorescence quantum yields $(\Phi_F)_v$, lifetimes τ_v, and radiative (k_r) and nonradiative (k_{nr}) decay rates of vibrational levels of $CF_4^+\ \tilde{C}\ ^2T_2$.

v_1	E/(eV)	CF_3^+/CF_2^+	$(\Phi_F)_v$[a]	τ_v/ns	k_r ($10^8\ s^{-1}$)[b]	k_{nr} ($10^8\ s^{-1}$)[c]
0	21.66	∞	1			
1	21.75	∞	1			
2	21.84	12±2	0.92±0.20	9.0±0.3	1.0±0.2	0.09±0.02
3	21.93	10.4±0.9	0.91±0.08			
4	22.02	6.9±0.4	0.87±0.04	8.6±0.4	1.01±0.07	0.15±0.01
5	22.11	4.5±0.1	0.82±0.02			
6	22.20	3.3±0.1	0.77±0.02	8.4±0.3	0.92±0.04	0.27±0.01
7	22.28	2.57±0.06	0.72±0.01			
8	22.36	1.69±0.03	0.63±0.01	7.9±0.4	0.80±0.03	0.47±0.02
9	22.44	1.54±0.03	0.61±0.01			
10	22.52	1.13±0.03	0.53±0.01			

[a]Calculated assuming the ratio of the CF_3^+ to CF_2^+ signal is $(\Phi_F)_v/[1-(\Phi_F)_v]$.
[b]Calculated from $k_r=(\Phi_F)_v/\tau_v$.
[c]Calculated from $k_{nr}=[1-(\Phi_F)_v]/\tau_v$.

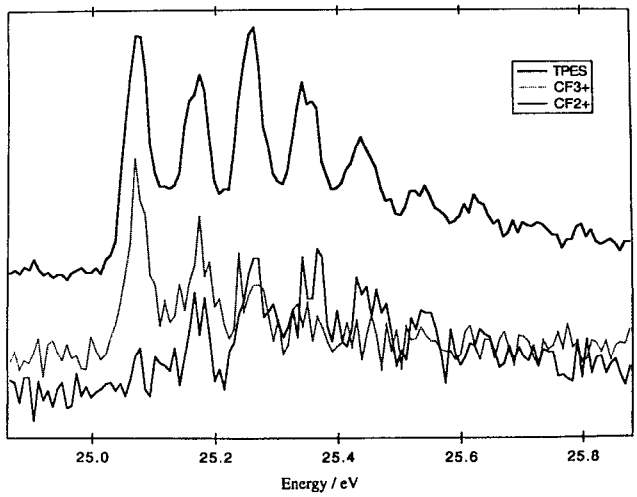

FIG. 4. Threshold photoelectron spectrum and coincidence yields of CF_2^+ and CF_3^+ from CF_4 between 24.9 and 25.8 eV. The photon resolution is 0.05 nm or ~0.026 eV.

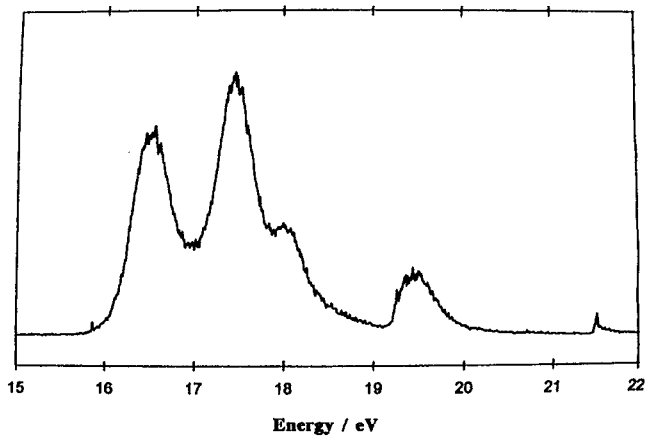

FIG. 5. Threshold photoelectron spectrum of SiF_4 between 15 and 22 eV recorded at a photon resolution of 0.1 nm or ~0.026 eV at 18 eV.

different vibrational intensity structure to the He II photoelectron band,[12] where direct ionization to $\nu_1=0$ is by far the strongest peak, and only very weak bands to $\nu_1>0$ are observed. This is a classic example of how autoionization, in this case via high-lying Rydberg states of CF_4 around 25 eV, can contribute by an indirect process to the threshold photoelectron signal, resulting in an anomalous non-Franck–Condon vibrational distribution. The CF_3^+ yield arises indirectly from radiative decay of the $\tilde{D}\ ^2A_1$ state of CF_4^+ to the repulsive $\tilde{A}$ state which dissociates directly to CF_3^++F, the CF_2^+ signal possibly via internal conversion into high vibrational levels of the $\tilde{C}\ ^2T_2$ state of CF_4^+ prior to direct dissociation. Figure 4 shows that there is vibrational state selectivity in this competition, with the radiative channel dominating at low values of ν_1, the nonradiative channel dominating at high values of ν_1. We obtain $(\Phi_F)_v=0.9$, 0.57, 0.36, 0.29, 0.18, 0.20, and 0.2 for $v_1=0$–6, respectively, and a vibrationally averaged value for the fluorescence quantum yield of 0.38 ± 0.02. Other than displaying the higher resolution that can be obtained with the McPherson monochromator, our conclusions from this TPEPICO spectrum are unchanged from those given in the lower-resolution study.[2] PIFCO and TPEFCO coincidence experiments on the $CF_4^+\tilde{D}$ state were not performed for two reasons. First, the partial photoionization cross section into this state is relatively small.[37] Second, its lifetime (2.1 ns)[38] is too short to be measured accurately in a fluorescence coincidence experiment with an optimum TDC resolution of 1 ns and a photomultiplier response time of 1.5 ns.

C. Silicon tetrafluoride

The He I and He II photoelectron spectra (PES) of SiF_4 have been reported in the literature.[11,12] The shape and structure of the first five bands is similar to that of CF_4, the four lowest bands are accessible with He I radiation and only the fifth band (ionization to $\tilde{D}\ ^2A_1$) needs the higher energy of He II radiation. As with CF_4, the first two bands are essentially continuous with no vibrational structure. The third band shows a small progression in ν_1, and the fourth band shows a longer progression in ν_1 with a satellite band to higher energy of each member being due to a combination band with one quantum of ν_4. The fifth band is very narrow, and no vibrational structure is resolved in the He II PES. To date, there has been no report of a TPES of SiF_4. Figure 5 shows a flux-normalized TPES from 15 to 22 eV recorded at a wavelength resolution of 0.1 nm. Two points are of note. First, the relative intensities of the first three bands (ionization to $SiF_4^+\tilde{X}$, $\tilde{A}$, and $\tilde{B}$) are approximately unchanged from those observed with the fixed-frequency lamp sources, but the fourth and fifth bands are much weaker in the threshold spectrum. Second, there is some evidence of additional structure in the high-energy tail of the $\tilde{B}\ ^2E$ band between 18.5 and 19.2 eV, and, unlike the He I and He II spectra, the threshold electron signal does not return to the baseline in this region. Such an effect has been observed in the TPES of CF_4,[33] and has been interpreted as evidence for autoionizing states of CF_4 in this energy region giving rise to a non-Franck–Condon distribution of vibrational levels in the $CF_4^+\tilde{B}$ photoelectron band. We have not investigated this phenomenon in the TPES of SiF_4 in detail, since the main purpose of this work was to study the state-selected fragmentation of the valence states of SiF_4^+ by coincidence techniques, but this effect warrants further study.

Using an electron–ion coincidence technique,[5] there has been only one previous study of the fragmentation of the outervalence states of SiF_4^+, but as described earlier there was no energy analysis of the photoelectrons in these experiments. Over the energy range 16–23 eV SiF_4^+ and SiF_3^+ were the only ions observed and their yield curves were obtained. SiF_2^+ was not observed. Due to the lack of energy analysis, it was not possible to say whether the fragmentation channels observed at each of the five valence states of SiF_4^+ were unique, and the data for the KE released were only of limited value. To date, there have been no reports of the fragmenta-

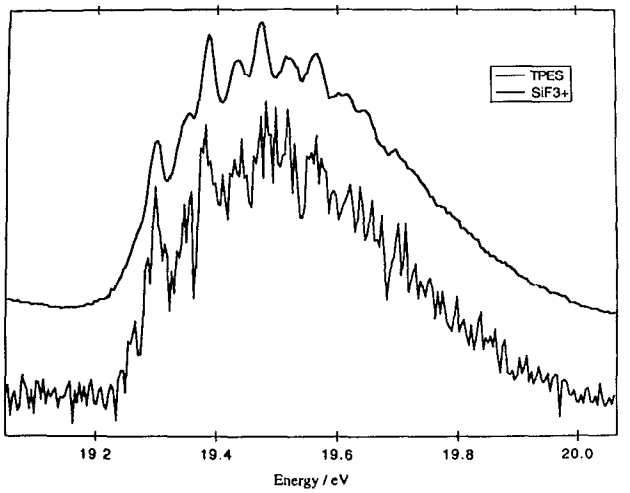

FIG. 6. Threshold photoelectron spectrum and coincidence yield of SiF_3^+ from SiF_4 between 19.1 and 20.0 eV. The photon resolution is 0.05 nm or ~0.015 eV.

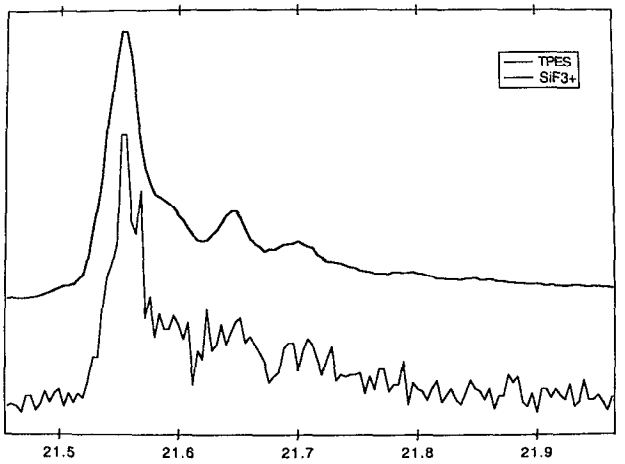

FIG. 7. Threshold photoelectron spectrum and coincidence yield of SiF_3^+ from SiF_4 between 21.5 and 21.9 eV. The photon resolution is 0.05 nm or ~0.018 eV.

tion of these valence states by coincidence techniques in which the energy of the photoelectron is defined.

In this study, as with CF_4^+, we have concentrated our effort to study the decay dynamics of the $\tilde{C}\ ^2T_2$ and $\tilde{D}\ ^2A_1$ states of SiF_4^+ by TPEPICO and TPEFCO spectroscopy. We have also measured the KE released into the fragment ions at the Franck–Condon maximum of the five valence states of SiF_4^+. Figure 6 shows the TPEPICO spectrum of the $\tilde{C}\ ^2T_2$ state of SiF_4^+ recorded in the energy-scanning mode. The resolution is 0.05 nm, or ~0.015 eV. SiF_3^+ is the only ion observed, and its yield and the TPE signal are displayed. The TPES is almost identical to the He I spectrum of Jadrny *et al.*,[11] showing that autoionization is not an important process over the energy range 19.2–20.0 eV. The major vibrational progression in the TPES is the ν_1 vibration, with each member having a satellite band to higher energy corresponding to one quantum of ν_4. The peak energies and assignments are given in Table II, we obtain an adiabatic IP of 19.302 ±0.006 eV, and values for ν_1 and ν_4 of 0.084±0.004 eV (677±32 cm^{-1}) and 0.052±0.004 eV (419±32 cm^{-1}), respectively. The value for the adiabatic IP is in exact agreement with that of Jadrny *et al.*, the values for the two vibrational wave numbers can be compared with values of ν_1=707±1 and ν_4=431±1 cm^{-1} obtained from a high-resolution optical study of the $\tilde{D}-\tilde{C}$ electronic transition in SiF_4^+.[39] The presence of bands involving the nontotally symmetric ν_4 mode of t_2 symmetry both in the TPES and the ion optical emission spectrum shows that the $\tilde{C}\ ^2T_2$ state of SiF_4^+ does not have tetrahedral symmetry but is showing Jahn–Teller distortion to C_{3v} geometry. Considering now the ion(s) that are observed in coincidence with threshold electrons, SiF_3^+ is the only fragment ion which is thermodynamically accessible to the $SiF_4^+\tilde{C}$ state (SiF_2^+ lies 1.6 eV higher in energy), and is therefore the only fragment ion observed (Fig. 6). Its yield matches directly that of the Franck–Condon determined TPE signal, with partial resolution of the vibrational structure that is observed in the TPES. Unlike the $\tilde{C}\ ^2T_2$ state of CF_4^+, the $\tilde{C}\ ^2T_2$ state of SiF_4^+ does not fluoresce with any appreciable quantum yield,[40] and therefore a radiative decay process cannot contribute to the ions observed in coincidence with threshold electrons. In particular, the $\tilde{C}-\tilde{X}$ transition in SiF_4^+ might access some parts of the $\tilde{X}$-state potential which are stable with respect to dissociation to SiF_3^++F (especially if the adiabatic IP of the $\tilde{X}$ state is as low as 15.29 eV, as Kickel *et al.*[27] suggest). Under these circumstances the SiF_4^+ ion would then be observed in coincidence with a threshold electron. This phenomenon is not observed, and is further evidence that the decay dynamics of the $\tilde{C}$ state of SiF_4^+ are dominated by nonradiative processes. The most likely decay route of $SiF_4^+\tilde{C}$ to SiF_3^+ is via internal conversion into the $\tilde{B}\ ^2E$ state, a process which will be assisted by dynamic Jahn–Teller distortion of the $\tilde{C}\ ^2T_2$ state to C_{3v} geometry. (A similar effect is observed for dissociation of the lowest Rydberg state of CH_4 $\tilde{A}\ ^1T_2$ into high vibrational levels of its ground state;[41] the main products of photodissociation of CH_4 at ~11 eV are CH_3+H, and not CH_2+H_2 as predicted.)[18] The $\tilde{B}$ state could then internally convert into a repulsive region of the $\tilde{A}$ state which dissociates directly to form SiF_3^++F. Further evidence for this mechanism comes from an analysis of the KE releases (see below).

Figure 7 shows the TPEPICO spectrum of the $\tilde{D}\ ^2A_1$ state of SiF_4^+ recorded in the energy-scanning mode at a resolution of 0.05 nm, or ~0.018 eV. Although SiF_2^+ is thermodynamically now accessible, again SiF_3^+ is the only ion observed, and its yield and the TPE signal are displayed. The TPES is very similar to the He II PES, showing a strong vertical transition to v=0 of this electronic state of the ion with little associated vibrational structure. The ν_1=1 band is observed for the first time in any kind of photoelectron spectrum, and we obtain ν_1=0.092±0.005 eV or 742±40 cm^{-1}, in excellent agreement with a value of 743.4±1.0 cm^{-1} from the $SiF_4^+\tilde{D}-\tilde{C}$ optical emission study.[39] Our value for the adiabatic IP, 21.554±0.007 eV, is in exact agreement with the value of 21.55 eV quoted by Lloyd and Roberts from the

He II PES.[12] Weak shoulders are observed on the high-energy sides of both $\nu_1=0$ and 1 in the TPES. These peaks, with energies of 21.586 and 21.700 eV, cannot be assigned to any further member of the allowed $\nu_1(a_1)$ progression. It seems that their most likely assignments are to $\nu_2(e)=1$ at 0.032 eV or 258 cm^{-1} and $\nu_3(t_2)=1$ at 0.146 eV or 1178 cm^{-1}, respectively. (Neutral SiF_4 has similar values of $\nu_2=268$ and $\nu_3=1031$ cm^{-1}.)[14] These "forbidden" peaks could then arise due to a second-order pseudo-Jahn–Teller interaction between the close-lying $\tilde{D}\ ^2A_1$ and $\tilde{C}\ ^2T_2$ states of SiF_4^+. Such an observation of forbidden vibrational structure in a nondegenerate photoelectron band has been observed in the He I PES of the $\tilde{X}\ ^2A_2'$ state of BF_3^+ caused by the nearby doubly degenerate $\tilde{B}\ ^2E'$ state which shows first-order Jahn–Teller splitting.[42] Figure 7 shows that the SiF_3^+ ion yield follows the TPE signal, with the $\nu_1=1$ peak being partially resolved in the ion yield spectrum. We believe that the predominant cause of the SiF_3^+ signal is from radiative decay of the $SiF_4^+\tilde{D}$ state via $\tilde{D}-\tilde{A}$ fluorescence to the repulsive $\tilde{A}$ state which dissociates directly to $SiF_3^+ + F$. The fluorescence quantum yield of the $\tilde{D}\ ^2A_1$ state of SiF_4^+ has not been measured, but the relative strength of the $\tilde{D}-\tilde{C}$ ion emission spectrum[39] and the invariance of the $\tilde{D}$-state lifetime (9.1 ns) with excitation energy[40] strongly suggests that a radiative process dominates the decay dynamics of this state and Φ_F is close to its maximum value of 1. If this is true, the fragment ions that are observed in coincidence with a threshold electron are a manifestation of the decay routes of the lower electronic states to which $\tilde{D}$-state fluorescence occurs. Therefore SiF_3^+ is the only fragment ion observed.

TPEFCO spectra were recorded at two energies within the $SiF_4^+\tilde{D}$ state Franck–Condon envelope, 21.55 and 21.65 eV, corresponding to $\nu_1=0$ and 1 (Fig. 8). The optical resolution was 0.04 eV, no filter was used with the photomultiplier tube, and a TDC resolution of 2 ns was used. The lifetimes of these two levels, τ_v, are independent of ν_1, and within experimental error take the same value of 9 ± 2 ns. The limited number of coincidences in each spectrum even after 12 h data collection is primarily a result of the small partial ionization cross section into the $\tilde{D}$ state of SiF_4^+,[43,44] a factor of ~8 smaller than the cross section into the $\tilde{C}$ state of CF_4^+;[37] this explains the much-improved signal-to-noise ratio of the $CF_4^+\tilde{C}$-state TPEFCO spectra (Fig. 3) after a comparable data accumulation time. The lifetimes agree with those obtained from time-resolved fluorescence experiments.[40] The advantage of the TPEFCO technique is that it measures the lifetime of an individual vibrational level, whereas a time-resolved fluorescence experiment measures a convolution of the lifetimes of all the vibrational levels which are energetically accessible. The results from the latter experiment[40] show that the $\tilde{D}$-state lifetime is independent of excitation energy, τ_v therefore is probably independent of vibrational level, and this result is indeed partially confirmed by the two TPEFCO experiments. In this particular case, the advantage of vibrational state selectivity is negated by the substantially reduced signal-to-noise ratio of the coincidence spectrum and essentially no new information is obtained from the TPEFCO experiments. A PIFCO experiment was not made at the $\tilde{D}\ ^2A_1$ state of SiF_4^+, but the result can be predicted with

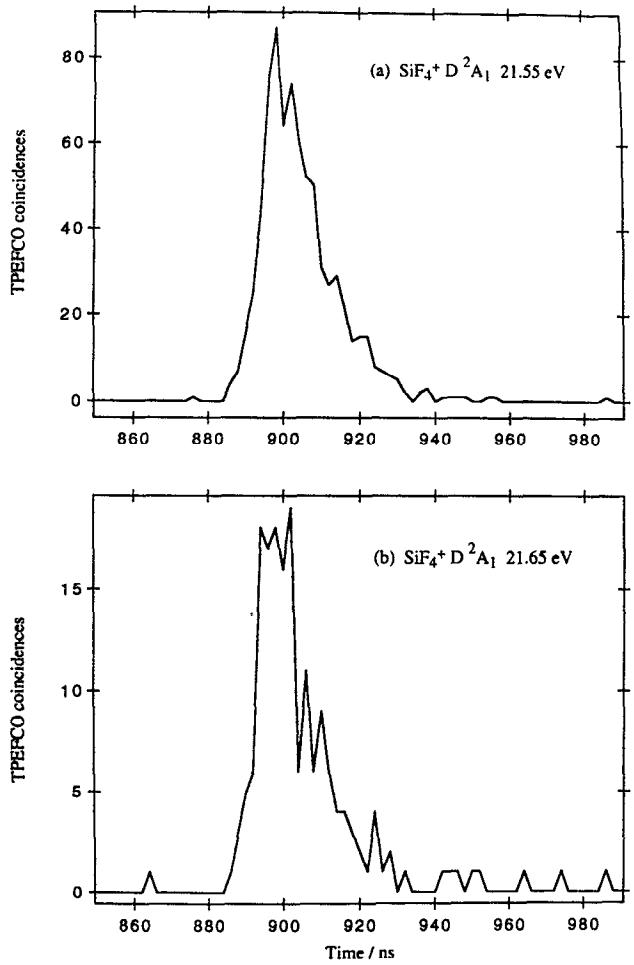

FIG. 8. TPEFCO spectra of the fluorescence from the $\tilde{D}\ ^2A_1$ state of SiF_4^+ at excitation energies of (a) 21.55, (b) 21.65 eV, corresponding to $\nu_1=0$ and 1, respectively. The photon resolution is 0.1 nm (~0.04 eV), the time resolution is 2 ns per channel, and the accumulation time of each spectrum is ~12 h.

a high degree of confidence. Since bound–free $\tilde{D}-\tilde{A}$ fluorescence centered at 304 nm dominates the emission spectrum of the $\tilde{D}$ state,[45] a coincidence signal would be observed with ions of $m/e=85$ (SiF_3^+), reflecting the repulsive nature of the $\tilde{A}$-state potential energy surface.

TPEPICO spectra at fixed photon energies were measured at the Franck–Condon maxima of the five valence states of SiF_4^+. A time resolution of 8 ns per channel was possible for all five measurements, and data accumulation times ranged from 2 h ($\tilde{A}$ state) to 8 h ($\tilde{D}$ state). Figure 9 shows the broadening of the SiF_3^+ peak at 21.55 eV, the maximum of the $SiF_4^+\tilde{D}$ state. Detailed KERDs and hence mean kinetic energy releases can be derived from an analysis of such TOF shapes.[8] The method used is to compute a set of TOF peaks (each with a discrete energy release ϵ_t) and fit this basis set to the experimental peak using a linear regression technique. The discrete energies are calculated by $\epsilon_t=(2n-1)^2\Delta E$ where $n=1,2,3,...$ and ΔE (the minimum release when $n=1$) depends primarily on the statistical quality of the data. In practice only mean KE releases can reli-

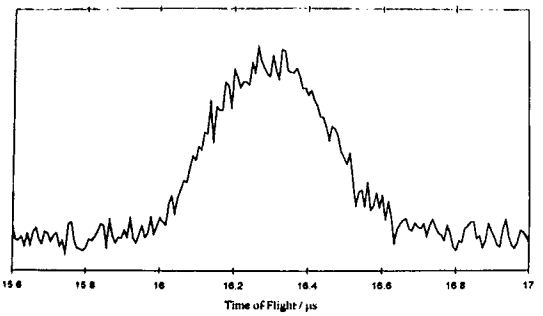

FIG. 9. Coincidence time-of-flight spectrum of SiF_3^+ from SiF_4 photoionized at 21.55 eV into the $\tilde{D}\ ^2A_1$ state of the parent ion. The time resolution is 8 ns per channel, and the accumulation time is ~8 h.

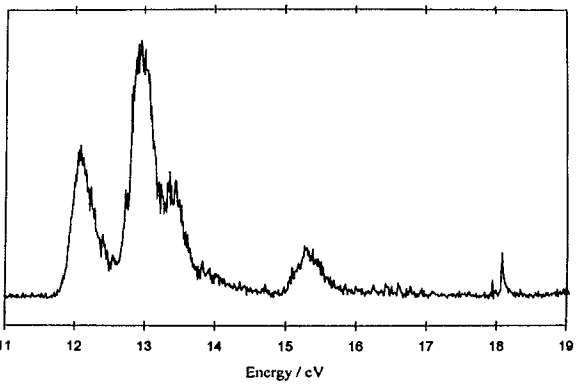

FIG. 10. Threshold photoelectron spectrum of $SiCl_4$ between 11 and 19 eV. The photon resolution is 0.1 nm or ~0.018 eV at 15 eV.

ably be obtained, the results are shown in Table IV, and in each case they are relatively insensitive to the form of the distribution. There are two related reasons for this. First, unfavorable kinematics; for $SiF_4^+ \rightarrow SiF_3^+ + F$ the daughter ion has over 80% of the mass of the parent ion. Second, there is no cooling of the translational temperature, T, of molecules along the axis of the TPEPICO apparatus since the molecules emerge from the inlet needle with little directionality.[1] With k_BT as high as 25 meV, this thermal effect broadens the TOF peak for each value of ϵ_t and degrades the detailed form of the TOF distribution. Such measurements have been made for the five valence states of CF_4^+ by us and others,[2,30–32] but these are the first such results for SiF_4^+. Two points are noted. First, the small value for the KE release from the $\tilde{X}$ state at 16.60 eV reflects the closeness of the $SiF_3^+ + F$ asymptote (16.2 eV). Even so, a release of 0.13 eV constitutes 32% of the available energy, implying that dissociation of this state is essentially nonstatistical with a large amount of the available energy being deposited into translation. Thus Franck–Condon photoionization of SiF_4^+ at 16.60 eV accesses a part of the ionic $\tilde{X}$-state surface which is predominantly repulsive. Second, the mean energy releases from the four excited valence states of SiF_4^+ are very similar with values between 0.52 and 0.65 eV. The $\tilde{A}$-state result means that 42% of the available energy is channeled into translational motion of the SiF_3^+ and F products, the high amount again being characteristic of a nonstatistical, direct dissociation process off a repulsive potential energy surface. The $\tilde{B}$- and $\tilde{C}$-state results suggest that these states evolve rapidly into the $\tilde{A}$ state by internal conversion (in the latter case assisted by Jahn–Teller distortion of the state), prior to dissociation off the $\tilde{A}$-state repulsive surface. The $\tilde{D}$-state result is compatible with a radiative process, in particular $\tilde{D}$–$\tilde{A}$ fluorescence, dominating the decay dynamics of this state.

TABLE IV. Mean kinetic energy releases from fragmentation of electronic states of SiF_4^+.

Daughter ion	State	Energy/eV	Mean KE_{trans}/eV[a]
SiF_3^+	$\tilde{X}\ ^2T_1$	16.60	0.13±0.04
SiF_3^+	$\tilde{A}\ ^2T_2$	17.50	0.54±0.03
SiF_3^+	$\tilde{B}\ ^2E$	18.04	0.52±0.03
SiF_3^+	$\tilde{C}\ ^2T_2$	19.46	0.65±0.04
SiF_3^+	$\tilde{D}\ ^2A_1$	21.55	0.59±0.05

[a]The quoted error is a measure of how each TOF distribution is fitted (see the text), rather than a true representation of the experimental uncertainty.

D. Silicon tetrachloride

Figure 10 shows a flux-normalized, survey TPES of $SiCl_4$ from 11 to 19 eV recorded at a wavelength resolution of 0.1 nm. This range spans the ground ($\tilde{X}$) and the four outervalence excited states ($\tilde{A}$–$\tilde{D}$) of $SiCl_4^+$. Similar features as in Fig. 10 have been observed by He I and II PES,[13] although the relative intensities of the five bands are rather different in the threshold spectrum; the $\tilde{A}$-state band is stronger, and the $\tilde{C}$- and $\tilde{D}$-state bands are weaker. Each band was studied under higher resolution (0.025–0.03 nm) in order to resolve possible vibrational structure, with effort being concentrated on the $\tilde{X}$, $\tilde{C}$, and $\tilde{D}$ ionic states [Figs. 11(a), 11(b), and 11(c), respectively]. Surprisingly, neither the $\tilde{X}$ nor $\tilde{C}$ states exhibit any structure at a resolution of 0.03 nm (corresponding to an energy of ~3 and 6 meV, respectively), despite the fact that the $\tilde{X}$ state is now known to be bound (see later) and the $\tilde{C}$ state is known to fluoresce.[46] However, the $\tilde{D}$ state, which is much narrower than either the $\tilde{X}$ or $\tilde{C}$ states in the survey spectrum, shows three resolved vibrational peaks when recorded at a resolution of 0.025 nm, with energies of 18.110, 18.157, and 18.201 eV [Fig. 11(c)]. The vibrational spacing of 47±2 meV or 379±16 cm^{-1} is assigned to the ν_1 totally symmetric Si–Cl stretch of $SiCl_4^+$. Unlike the $\tilde{D}$ state of SiF_4^+ (Sec. IV C), there is no evidence for any other vibrational mode being active at this resolution. Our value for ν_1 can be compared with that obtained from a He I PES (36 meV or 290 cm^{-1})[13] taken at lower resolution than the present TPES measurements, and a value of 52.4 meV (423 cm^{-1})[14] for the corresponding vibrational interval in neutral $SiCl_4$. The slight decrease in ν_1 upon ionization to the $\tilde{D}$ state probably reflects a slight increase in the Si–Cl bond distance.

TPEPICO spectra in the energy-scanning mode were recorded over these five states ($\tilde{X}$–$\tilde{D}$) and the first innervalence state ($\tilde{E}\ ^2T_2$) of $SiCl_4^+$ at a resolution of 0.1 nm. The $\tilde{X}$-, $\tilde{A}$-, and $\tilde{B}$-state data are presented in Fig. 12, the $\tilde{C}$-, $\tilde{D}$-,

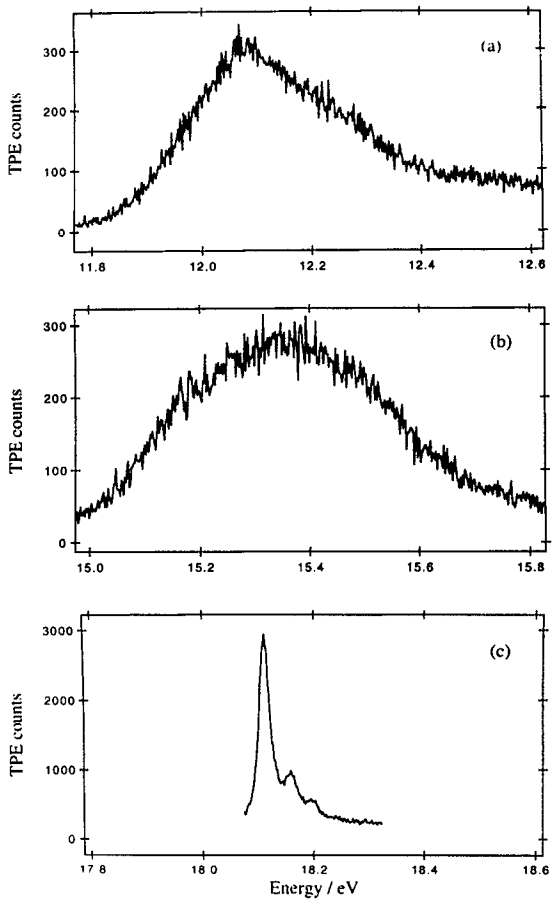

FIG. 11. (a) Threshold photoelectron spectrum of the $\tilde{X}\ ^2T_1$ state of $SiCl_4^+$ recorded at a resolution of 0.03 nm or ~3 meV. (b) Threshold photoelectron spectrum of the $\tilde{C}\ ^2T_2$ state of $SiCl_4^+$ recorded at a resolution of 0.03 nm or ~6 meV. (c) Threshold photoelectron spectrum of the $\tilde{D}\ ^2A_1$ state of $SiCl_4^+$ recorded at a resolution of 0.025 nm or ~6 meV.

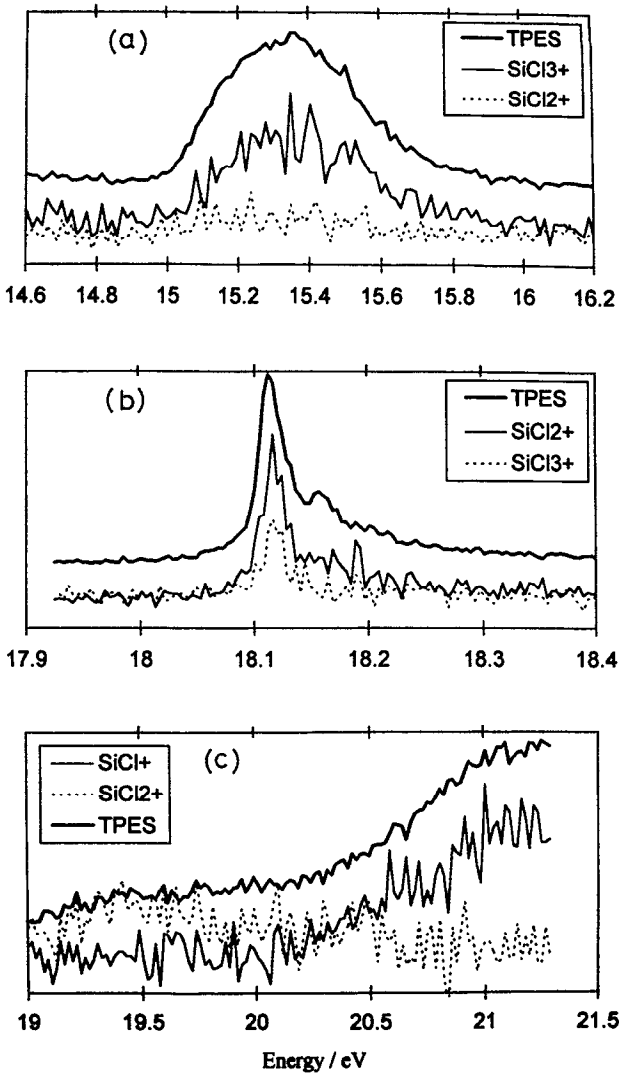

FIG. 13. (a) Threshold photoelectron spectrum and coincidence yields of $SiCl_3^+$ and $SiCl_4^+$ from $SiCl_4$ between 14.6 and 16.2 eV. (b) Threshold photoelectron spectrum and coincidence yields of $SiCl_2^+$ and $SiCl_3^+$ from $SiCl_4$ between 17.9 and 18.4 eV. (c) Threshold photoelectron spectrum and coincidence yields of $SiCl^+$ and $SiCl_2^+$ from $SiCl_4$ between 19.0 and 21.5 eV. In all cases the photon resolution is 0.1 nm.

and $\tilde{E}$-state data in Figs. 13(a), 13(b), and 13(c), respectively. Figure 12 shows that below 14.5 eV the $SiCl_3^+$ and $SiCl_4^+$ ions are observed. The $SiCl_4^+$ ion yield matches the TPE signal for the region 11.5–12.5 eV (the Franck–Condon zone

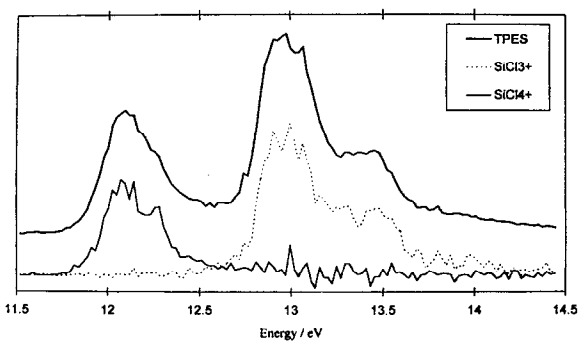

FIG. 12. Threshold photoelectron spectrum and coincidence yields of $SiCl_3^+$ and $SiCl_4^+$ from $SiCl_4$ between 11.5 and 14.5 eV. The photon resolution is 0.1 nm or ~0.014 eV.

of the ionic $\tilde{X}$ state), whereas the $SiCl_3^+$ yield follows the TPE signal for the region 12.7–14.5 eV (the Franck–Condon zones of the $\tilde{A}$ and $\tilde{B}$ states). The $SiCl_4^+$ result confirms what is to be expected from the thermodynamics of this system (Table I), that is, the ground state of $SiCl_4^+$ is bound since its adiabatic and vertical IPs (11.8 and 12.1 eV, respectively) lie below the $SiCl_3^+ + Cl$ dissociation channel at 12.7 eV. The $SiCl_3^+$ signal in the TPEPICO spectrum clearly originates from fragmentation of the $\tilde{A}$ and $\tilde{B}$ states of $SiCl_4^+$, with the threshold for $SiCl_3^+$ production coinciding with the adiabatic IP of the $\tilde{A}$ state. Thus those regions of the $\tilde{A}$- and $\tilde{B}$-state surfaces populated by Franck–Condon photoionization are repulsive in nature. These results also confirm mass spectrometric studies[47] which show that both $SiCl_3^+$ *and* $SiCl_4^+$ are major ion products in the electron impact ionization of $SiCl_4$. For the $\tilde{C}$, $\tilde{D}$, and $\tilde{E}$ states of $SiCl_4^+$, there is no simple

correlation between an ionic state and production of one fragment ion. Thus the $\tilde{C}\ ^2T_2$ state produces both $SiCl_3^+$ and $SiCl_4^+$ in the ratio of ~4:1 [Fig. 13(a)], the $\tilde{D}\ ^2A_1$ state produces $SiCl_2^+$ and $SiCl_3^+$ also in the ratio of ~4:1 [Fig. 13(b)], and the $(1t_2)^{-1}\tilde{E}\ ^2T_2$ innervalence state with an adiabatic IP of 20.0 eV[3] produces predominantly $SiCl^+$ and just possibly $SiCl_2^+$ in addition [Fig. 13(c)]. The results for the $\tilde{X}$, $\tilde{A}$, and $\tilde{B}$ ionic states, while easily predictable, have never been observed before, results for the $\tilde{C}$, $\tilde{D}$, and $\tilde{E}$ states have been observed at lower signal-to-noise ratio and inferior resolution in our previous study with the Seya monochromator.[3] One fixed-energy high time resolution TPEPICO spectrum was recorded in our earlier work[3] at the $\tilde{C}$ state of $SiCl_4^+$ to measure the KE release into the $SiCl_3^+ + Cl$ channel (~0.4 eV). No further KERDs have been measured in this study, primarily because the earlier study showed that the multiple isotopes of the silicon and chlorine atoms degrade the information that can be obtained from such spectra.

The $\tilde{C}$ state of $SiCl_4^+$ decays radiatively,[46] a nonstatistical process in such a five-atom polyatomic ion composed of heavy atoms, and both PIFCO and TPEFCO spectra have been recorded at the Franck–Condon maximum of this state, 15.36 eV. Fluorescence occurs both to the bound ground state of the ion and to the repulsive first excited state. Figure 14 shows three PIFCO spectra each recorded with a time resolution of 128 ns per channel. In Fig. 14(a) no filter is used in front of the photomultiplier tube, in Fig. 14(b) a Schott UG5 filter transmitting the range 220–400 nm is used, and in Fig. 14(c) a Schott OG515 filter transmitting wavelengths greater than 500 nm is used. In Fig. 14(a) coincidences are observed with two ions whose mass-to-charge ratio corresponds to $SiCl_3^+$ and $SiCl_4^+$, in Fig. 14(b) only coincidences with $SiCl_4^+$ are observed, and in Fig. 14(c) only coincidences with $SiCl_3^+$ are observed. These PIFCO measurements confirm that the final states of the two radiative processes originating from the $\tilde{C}$ state of $SiCl_4^+$ differ significantly; one process results in a stable state of the parent ion ($\tilde{X}$) while the other process produces the unstable $\tilde{A}$ state which fragments to $SiCl_3^+ + Cl$. In an earlier optical study with a resolution of 0.2 nm[46] using electron-impact ionization of a supersonic beam of $SiCl_4$, two broad bands were observed with peaks at 410 and 570 nm. They were assigned to $SiCl_4^+$ $\tilde{C}-\tilde{X}$ and $\tilde{C}-\tilde{A}$, respectively, and both bands appeared to be continuous in nature. This PIFCO study shows that the radiative process involving the UV emission must be interpreted as a bound–bound transition which has the appearance of a bound–free transition due to rovibronic spectral congestion. Indeed, a more detailed study of the two bands at close to Doppler-limited resolution shows a clear difference between them; the visible band is continuous in nature, while the UV band has a large amount of discrete structure.[48] In our TPEPICO measurement the ions $SiCl_3^+$ and $SiCl_4^+$ are detected with equal efficiencies, and the 4:1 intensity ratio presumably reflects the relative values of the electronic moments of the $\tilde{C}-\tilde{A}$ and $\tilde{C}-\tilde{X}$ transitions. In the PIFCO experiment with no filter [Fig. 14(a)] the similar intensities of the signals due to $SiCl_3^+$ and $SiCl_4^+$ reflect the convolution of this effect with the reduced quantum efficiency of the photomultiplier tube in the red region of the visible (where $\tilde{C}-\tilde{A}$ emission occurs) compared to that in the UV/blue visible (where $\tilde{C}-\tilde{X}$ emission occurs).

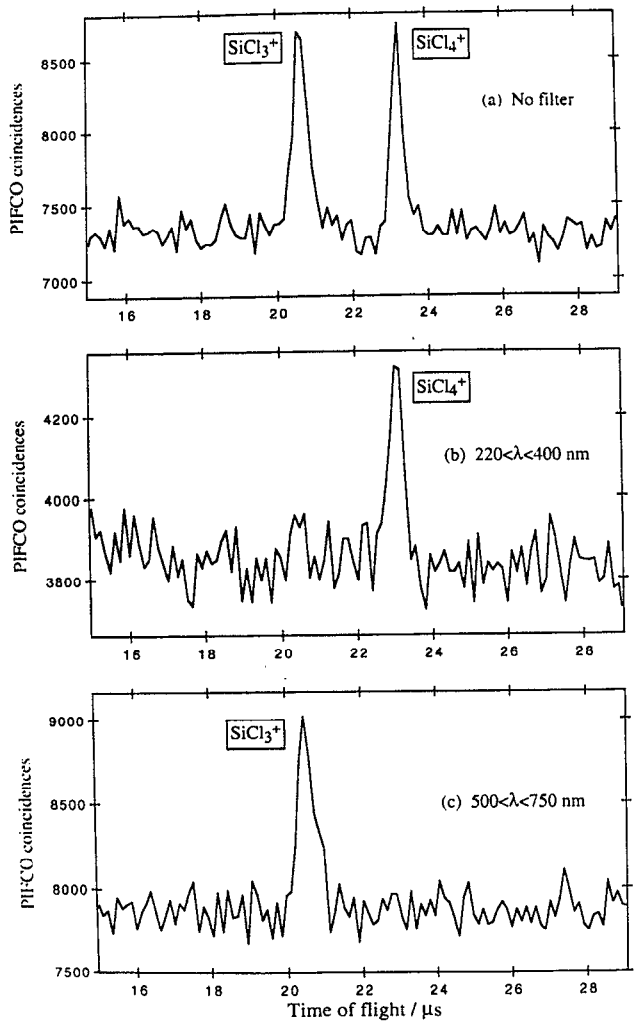

FIG. 14. PIFCO time-of-flight spectra of the fluorescence from the $\tilde{C}\ ^2T_2$ state of $SiCl_4^+$ at 15.36 eV. The time resolution is 128 ns per channel and the accumulation time is ~8 h for each spectrum. In (a) no optical filter, in (b) a Schott UG5 filter transmitting the range 220–400 nm, and in (c) a Schott OG515 filter transmitting wavelengths greater than 500 nm is used with the Mullard 2254 QB photomultiplier tube.

The strong fluorescence signal from the $\tilde{C}$ state of $SiCl_4^+$ allowed us, in addition, to record a TPEFCO spectrum. Figure 15 shows the spectrum recorded at an energy of 15.36 eV (the vertical IP) with a time resolution of 2 ns per channel and with no optical filter. The decay of the fluorescence signal can be fitted to a single exponential with a rate constant of $2.6\times10^7\ s^{-1}$, corresponding to a lifetime of 38 ns for the vibrational level(s) at the Franck–Condon maximum. This result is in excellent agreement with the value of 38.4 ns determined by a time-resolved fluorescence study.[40] The observation of radiative decay and the corresponding long lifetime strongly suggests that the fluorescence quantum yield of the $\tilde{C}$ state is close to unity, implying that internal conversion of this state into lower-lying electronic states of $SiCl_4^+$ is slow and inefficient. It is therefore very surprising that no

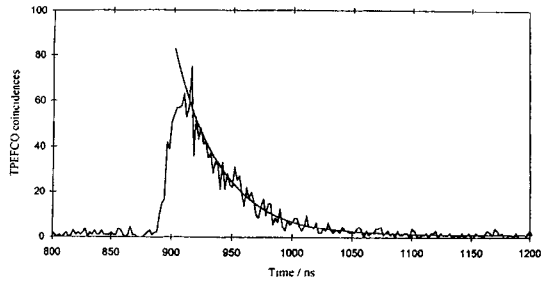

FIG. 15. TPEFCO spectrum of the fluorescence from the $\tilde{C}\ ^2T_2$ state of $SiCl_4^+$ at 15.36 eV. The time resolution is 2 ns per channel, the accumulation time is ~10 h, and no optical filter is used. A single exponential is drawn through the data with a rate constant of $2.6\times10^7\ s^{-1}$, corresponding to a lifetime of 38 ns.

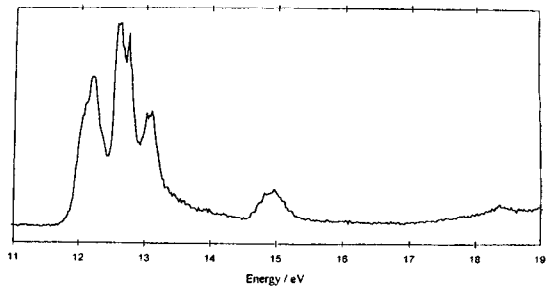

FIG. 16. Threshold photoelectron spectrum of $GeCl_4$ between 11 and 19 eV. The photon resolution is 0.1 nm or ~0.02 eV at 15 eV.

vibrational structure is resolved in the TPES even at a resolution of 6 meV [Fig. 11(b)]. Since the $\tilde{C}$-state lifetime is as long as 38 ns, predissociation or dissociation lifetime broadening cannot explain this absence of structure, and we can only conclude that spectral congestion caused by several vibrational modes being excited and/or spin–orbit effects is the cause of the continuous band. If the $\tilde{C}\ ^2T_2$ state retains tetrahedral symmetry, then only the $\nu_1(a_1)$ totally symmetric vibrational mode should be observed (as with $CF_4^+\tilde{C}$), and at a resolution of 6 meV a progression in this mode should be resolved even if ν_1 is substantially reduced from its value in neutral $SiCl_4$ of 52.4 meV. Therefore we conclude that nonsymmetric vibrational modes including one or more of $\nu_2(e)$, $\nu_3(t_2)$, and $\nu_4(t_2)$ (whose values in the neutral molecule are 18.5, 76.9, and 27.3 meV, respectively)[14] must be active. This then suggests that the ionic $\tilde{C}$ state is affected by Jahn–Teller distortion (as in the case of $SiF_4^+\tilde{C}$), and makes the observation of radiative decay from the $\tilde{C}$ state all the more surprising.

By analogy with the $\tilde{D}\ ^2A_1$ states of CF_4^+ and SiF_4^+,[34,36,39,45,49] it might be expected that the $\tilde{D}$ state of $SiCl_4^+$ also shows radiative decay via $\tilde{D}-\tilde{A}$ and $\tilde{D}-\tilde{C}$ emission. If this is so, then the $\tilde{D}-\tilde{A}$ channel could provide an (indirect) route for production of $SiCl_3^+$, the very weak minor channel observed. However, a TPEFCO experiment at an energy of 18.11 eV without any optical filter in front of the photomultiplier tube yielded negligible coincidence counts after 8 h of accumulation time. We conclude that the fluorescence quantum yield of this state is very small (probably less than 0.01), and nonradiative processes dominate. Since vibrational structure is resolved in the TPES of the $\tilde{D}$ state, fragmentation processes must occur at a rate less than 10^{13} s^{-1}, but in order to explain the negligible fluorescence yield the decay rate must be faster than $10^{10}\ s^{-1}$. The principle daughter ion produced from this state is $SiCl_2^+$, and we note that the threshold for production of this ion (18.1 eV) lies nearly 3 eV above its lowest thermodynamic threshold. This is another example of nonstatistical behavior in this family of molecular ions, since fragmentation to other daughter ions which are energetically allowed (e.g., $SiCl^+$ and $SiCl_3^+$) is scarcely observed. As with fragmentation of the $\tilde{C}$ state of CF_4^+ to $CF_2^+ + F_2$ or F+F, it is not possible to say whether the other products from the $\tilde{D}$ state of $SiCl_4^+$ are Cl_2 or Cl+Cl, and if the latter is the predominant channel, whether the dissociation is concerted (i.e., $SiCl_4^+\tilde{D}\rightarrow SiCl_2^+ + Cl + Cl$) or sequential (i.e., $SiCl_4^+\tilde{D}\rightarrow SiCl_3^+ + Cl \rightarrow SiCl_2^+ + Cl + Cl$). The threshold for $SiCl^+$ production (20.0 eV) [Fig. 13(c)] lies 3.2 eV above the lowest thermochemical channel producing this ion. This could correspond to the energy of the $\tilde{E}\ ^2T_2$ first innervalence state of $SiCl_4^+$, and again this represents another nonstatistical dissociation process.

E. Germanium tetrachloride

Figure 16 shows a TPES of $GeCl_4$ from 11 to 19 eV recorded at a resolution of 0.1 nm. Again, as in $SiCl_4^+$, the relative intensities of the peaks are slightly different from those recorded under nonthreshold conditions;[13] the main differences are that the $\tilde{A}$-state band is stronger and the $\tilde{D}$-state band is weaker under threshold conditions. The TPES is very similar to that of $SiCl_4$ (Fig. 10), but with two noticeable differences. First, a doublet is clearly resolved in the second band of $GeCl_4$ (ionization to $\tilde{A}\ ^2T_2$), and we assign this to spin–orbit splitting in this state. The magnitude of the splitting (155 meV or 1255 cm^{-1}) is compatible with both the Ge and the four Cl atoms making atomic contributions to the molecular splitting, and since the lower-energy band at 12.5 eV has the greater integrated intensity this strongly suggests that the sign of the molecular spin–orbit splitting constant is negative, as expected for a $(t_2)^5$ electron configuration.[50] The absence of a splitting in the $\tilde{A}\ ^2T_2$ band of $SiCl_4^+$ suggests that the very much smaller atomic contribution of Si $3p$ (153 cm^{-1}) compared to Ge $4p$ (960 cm^{-1}) is a significant factor. Second, the fifth band in the TPES (ionization to $GeCl_4^+\tilde{D}\ ^2A_1$) in much weaker than the corresponding band in $SiCl_4^+$; this fact is also observed in the He I spectra. The signal-to-noise ratio of this TPES of $GeCl_4$ is superior to that of previous He I spectra,[13] and in Table I we quote improved adiabatic IPs for the $\tilde{X}$, $\tilde{A}$, and $\tilde{B}$ states, all reduced by ~0.2 eV. No higher-resolution TPES studies were carried out.

TPEPICO spectra in the energy-scanning mode were recorded over the $\tilde{X}-\tilde{B}$ states [Fig. 17(a)] and the $\tilde{C}$ state [Fig. 17(b)] of $GeCl_4^+$ at a resolution of 0.1 nm. Due to the very small partial ionization cross section into the $\tilde{D}$ state under threshold conditions, this state was not studied. The picture

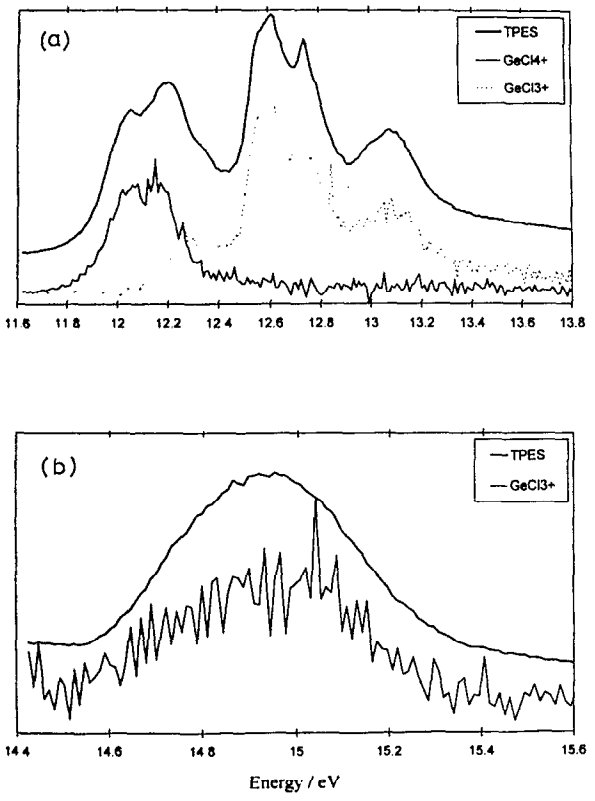

FIG. 17. (a) Threshold photoelectron spectrum and coincidence yields of $GeCl_3^+$ and $GeCl_4^+$ from $GeCl_4$ between 11.6 and 13.8 eV. The photon resolution is 0.1 nm or ~0.013 eV. (b) Threshold photoelectron spectrum and coincidence yield of $GeCl_3^+$ from $GeCl_4$ between 14.4 and 15.6 eV. The photon resolution is 0.1 nm or ~0.018 eV.

for the $\tilde{X}-\tilde{B}$ states is similar to that in $SiCl_4^+$. $GeCl_3^+$ and $GeCl_4^+$ are observed. The $GeCl_4^+$ yield matches the threshold photoelectron signal for most of the Franck–Condon region of the $\tilde{X}$ state, the $GeCl_3^+$ yield follows the TPE signal over the $\tilde{A}$ and $\tilde{B}$ states. The threshold for $GeCl_3^+$ production is 12.10 ± 0.03 eV, almost identical to the appearance potential from electron–impact mass spectrometry.[16] This energy is close to the vertical IP of the $GeCl_4^+$ $\tilde{X}$ state, and the yield of the trichloride ion rises as that of the parent ion falls. As with $SiCl_4^+$, these results are not surprising, given the thermodynamics of the system. Approximately half the Franck–Condon region of the $GeCl_4^+\tilde{X}$ state lies below the $GeCl_3^+ + Cl$ thermochemical limit, and these vibrational levels are stable with respect to dissociation. Higher vibrational levels lie above the dissociation limit and fragment to the trichloride ion. All levels of the $\tilde{A}$ and $\tilde{B}$ states lie above 12.10 eV, the $\tilde{A}$ state dissociates directly off a repulsive surface, the $\tilde{B}$ state probably indirectly via internal conversion through the $\tilde{A}$ state. These results have not been observed before, but as with $SiCl_4^+\tilde{X}-\tilde{B}$ they are not difficult to predict. However, given these results it is very surprising that the parent ion is not observed at all in a 70 eV electron–impact mass spectrum of $GeCl_4$.[47] The TPEPICO spectrum from the $\tilde{C}$ state [Fig. 17(b)] shows that $GeCl_3^+$ is the only ion observed and its yield follows the TPE signal. Despite the fact that the channel to $GeCl_2^+$ is energetically open, neither this ion nor the parent ion are observed.

As with $SiCl_4^+$, the $\tilde{C}$ state of $GeCl_4^+$ decays radiatively via $\tilde{C}-\tilde{X}$ and $\tilde{C}-\tilde{A}$ emission,[40,46] its lifetime is 65.4 ns, and a PIFCO spectrum has been recorded from this state. The spectrum recorded at the Franck–Condon maximum of 14.9 eV with a time resolution of 128 ns per channel and no optical filter shows coincidences only with $GeCl_3^+$. This result suggests either that $\tilde{C}-\tilde{A}$ fluorescence is much stronger than $\tilde{C}-\tilde{X}$ fluorescence in $GeCl_4^+$ or $\tilde{C}-\tilde{X}$ emission predominantly populates those parts of the $\tilde{X}$-state surface above the $GeCl_3^+ + Cl$ dissociation energy or both. All the points made in Sec. IV D about the absence or presence of Jahn–Teller effects in the $\tilde{C}$ state of $SiCl_4^+$ are pertinent to any discussion of the dynamics of the $\tilde{C}$ state of $GeCl_4^+$. Even though a high-resolution TPES of this state was not recorded, it is safe to predict that if spectral congestion is the cause of the absence of structure in the $SiCl_4^+\tilde{C}$-state TPE band, then this effect will be an even greater problem with the heavier $GeCl_4^+$ ion.

V. CONCLUSIONS

We have recorded TPEPICO spectra in the energy-scanning mode over the ground and the outervalence excited electronic states of four group IV tetrahalide ions, CF_4^+, SiF_4^+, $SiCl_4^+$, and $GeCl_4^+$, and have established which daughter ions are produced from fragmentation of each electronic state. Results for CCl_4^+ have been reported elsewhere.[3] For some of the excited states which decay radiatively by photon emission, PIFCO and TPEFCO spectra have been recorded at fixed photon energies. The important conclusions from these results are as follows.

(a) The behavior of the ground state of the molecular ion (MX_4^+) depends upon the energy of its adiabatic IP compared to that of the lowest dissociation channel (to $MX_3^+ + X$). In CF_4^+, all regions of the ground state populated by Franck–Condon photoionization lie on repulsive parts of the potential, in $SiCl_4^+$ the majority of the ground-state surface is bound, and in SiF_4^+ and $GeCl_4^+$ the situation is in between these two limits. Thus the parent ion is observed as a major product in ionization studies of $SiCl_4$ (this work), as a minor product in studies of $GeCl_4$ (this work) and SiF_4,[5] and not at all in studies of CF_4.[2,5] Vibrational structure has not been resolved in any ground-state photoelectron spectrum.

(b) The parts of the $\tilde{A}\ ^2T_2$ state potential energy surface populated by Franck–Condon photoionization are repulsive for all four ions, and all dissociate to $MX_3^+ + X$. Again, no structure has been resolved by photoelectron spectroscopy. The $\tilde{B}\ ^2E$ state of the ions all produce $MX_3^+ + X$ (this is the only fragment ion energetically accessible), but now vibrational structure has been observed in the photoelectron band in CF_4^+ [10,33] and SiF_4^+.[11] It is assumed that MX_3^+ is produced by internal conversion of $\tilde{B}\ ^2E$ into high vibrational levels of $\tilde{A}\ ^2T_2$, and this process occurs at such a rate that vibrational structure can still be resolved in the photoelectron band; this implies a rate for internal conversion of $\sim10^{11}-10^{13}\ s^{-1}$.

(c) The $\tilde{C}\ ^2T_2$ state of the four titled ions shows very different dynamical decay properties. In the $\tilde{C}$ state of CF_4^+, no Jahn–Teller distortion modes are active, and there is com-

petition between radiative decay (which indirectly produces CF_3^+) and fragmentation to CF_2^+. The relative yields of the two channels change with vibrational quantum number, and, from measurements of fluorescence quantum yields and lifetimes, rates for k_r and k_{nr} have been obtained as a function of v_1, the quantum number for the symmetric C–F stretch. The $\tilde{C}\ ^2T_2$ state of SiF_4^+ shows Jahn–Teller activity in ν_4 in the photoelectron band, radiative decay is not observed from this state, and we assume that the $\tilde{C}$-state distortion to C_{3v} symmetry "drives" internal conversion into the $\tilde{B}$, then $\tilde{A}$ states which dissociate to SiF_3^+. In the $\tilde{C}$ state of $SiCl_4^+$ and $GeCl_4^+$ radiative decay dominates, and the ions that are observed in the TPEPICO spectra are a manifestation of the *lower* electronic states to which photon emission from the $\tilde{C}$ state occurs. The absence of resolved vibrational structure in the $\tilde{C}$-state photoelectron bands of these two ions is surprising, and can only be explained by congested vibrational and/or spin–orbit structure.

(d) The $\tilde{D}\ ^2A_1$ state of all four ions under study also shows very different decay dynamics. In CF_4^+, both radiative decay (resulting indirectly in production of CF_3^+) and dissociation to CF_2^+ is observed, and again the branching ratio between these processes shows vibrational state selectivity; fluorescence dominates for low values of v_1, fragmentation for high values. Only SiF_3^+ is produced from the $\tilde{D}$ state of SiF_4^+, and since it is known that this state decays radiatively via $\tilde{D}$–$\tilde{A}$ emission,[39,45] we conclude that radiative decay is the dominant process from all parts of the $\tilde{D}$-state potential surface populated by photoionization. In $SiCl_4^+$ fragmentation to $SiCl_2^+$ dominates and radiative decay is a negligible channel. The $\tilde{D}$ state of $GeCl_4^+$ was not studied in this work due to the very weak threshold photoelectron signal, but in our previous study with no electron energy analysis[5] and hence a correspondingly stronger electron signal, fragmentation to both $GeCl^+$ and $GeCl_2^+$ was observed. Again, radiative decay is a very minor channel.

(e) Dynamical, rather than statistical, considerations are clearly dominating the fragmentation of the valence states of CF_4^+, SiF_4^+, $SiCl_4^+$, and $GeCl_4^+$. Almost certainly, this arises because of the instability of a large part of the ground-state surface of MX_4^+ which is accessed by Franck–Condon ionization of MX_4. In such a situation it is not appropriate to calculate a density of vibrational levels in order to determine a statistical fragmentation pattern. Thus a daughter ion does not appear at its thermochemical energy (which would be the case for statistical fragmentation patterns) but at the higher energy of an excited electronic state of the parent ion which correlates either adiabatically or diabatically to that ion. For example, the $\tilde{D}$ state of $SiCl_4^+$ fragments almost exclusively to $SiCl_2^+$, and fragmentation to other daughter ions which are energetically allowed (e.g., $SiCl^+$ and $SiCl_3^+$) is scarcely observed. As mentioned in Sec. IV D, radiative decay is another manifestation of nonstatistical behavior in excited states of these five-atom molecular ions. Since dynamical processes are dominant, a complete understanding of these results needs detailed potential energy surfaces for the ground and excited states of these ions, and how these surfaces evolve both adiabatically and diabatically into production of daughter ions. Parts of the potential energy surfaces have been calculated for the ground and excited states of CF_4^+ and SiF_4^+,[51] especially those parts near the minima, but the more difficult calculations of the evolution of these states along the dissociation coordinates or for the heavier tetrachloride species have not yet been carried out.

ACKNOWLEDGMENTS

We thank the staff at the Daresbury Laboratory for help, Dr I. Powis (Nottingham University) for the use of his kinetic energy analysis program, and Dr A. J. Yencha for a preprint of Ref. 33. SERC is thanked for an equipment grant, an Advanced Fellowship (P.A.H.), a Post-Doctoral Fellowship (D.M.S.), and a Research Studentship (K.R.Y.). R.P.T. and M.S. thank the British Council for a bilateral travel grant between Birmingham and Krakow Universities.

[1] P. A. Hatherly, M. Stankiewicz, K. Codling, J. C. Creasey, H. M. Jones, and R. P. Tuckett, Meas. Sci. Tech. **3**, 891 (1992).
[2] J. C. Creasey, H. M. Jones, D. M. Smith, R. P. Tuckett, P. A. Hatherly, K. Codling, and I. Powis, Chem. Phys. **174**, 441 (1993).
[3] D. M. Smith, R. P. Tuckett, K. R. Yoxall, K. Codling, and P. A. Hatherly, Chem. Phys. Lett. **216**, 493 (1993).
[4] P. A. Hatherly, K. Codling, D. M. Smith, R. P. Tuckett, K. R. Yoxall, and J. F. M. Aarts, Chem. Phys. **174**, 453 (1993).
[5] J. C. Creasey, I. R. Lambert, R. P. Tuckett, K. Codling, L. J. Frasinski, P. A. Hatherly, M. Stankiewicz, and D. M. P. Holland, J. Chem. Phys. **93**, 3295 (1990).
[6] W. C. Wiley and I. H. McLaren, Rev. Sci. Instrum. **26**, 1150 (1955).
[7] P. Baltzer, Phys. Rev. A **45**, 4374 (1992).
[8] I. Powis, P. I. Mansell, and C. J. Danby, Int. J. Mass Spectrosc. Ion Phys. **32**, 15 (1979).
[9] R. P. Tuckett, Chem. Soc. Rev. **19**, 439 (1990).
[10] C. R. Brundle, M. B. Robin, and H. Basch, J. Chem. Phys. **53**, 2196 (1970).
[11] R. Jadrny, L. Karlsson, L. Mattsson, and K. Siegbahn, Chem. Phys. Lett. **49**, 203 (1977).
[12] D. R. Lloyd and P. J. Roberts, J. Electron Spectrosc. **7**, 325 (1975).
[13] J. C. Green, M. L. H. Green, P. J. Joachim, A. F. Orchard, and D. W. Turner, Phil. Trans. R. Soc., London, Ser. A **268**, 111 (1970). P. J. Bassett and D. R. Lloyd, J. Chem. Soc. A **641**, (1971). R. G. Egdell, I. L. Fragala, and A. F. Orchard, J. Electron. Spectrosc. Relat. Phenom. **17**, 267 (1979).
[14] M. W. Chase, C. A. Davies, J. R. Downey, D. J. Frurip, R. A. MacDonald, and A. N. Syverud, J. Phys. Chem. Ref. Data **14**, Suppl. (1985).
[15] E. R. Fisher, B. L. Kickel, and P. B. Armentrout, J. Phys. Chem. **97**, 10204 (1993).
[16] J. Tamas, G. Czira, A. K. Maltsev, and O. M. Nefedov, J. Organometal. Chem. **40**, 311 (1972). O. Uy Manuel, D. W. Muenow, and J. L. Margrave, Trans. Faraday Soc. **65**, 1296 (1969).
[17] E. R. Fisher and P. B. Armentrout, Int. J. Mass Spectrom. Ion Process. **101**, R1 (1990).
[18] J. M. Dyke, L. Golab, N. Jonathan, A. Morris, and M. Okuda, J. Chem. Soc. Faraday Trans. 2 **70**, 1828 (1974).
[19] J. M. Dyke, A. E. Lewis, and A. Morris, J. Chem. Phys. **80**, 1382 (1984).
[20] N. P. C. Westwood, Chem. Phys. Lett. **25**, 558 (1974).
[21] G. Bosser, H. Bredohl, and I. Dubois, J. Mol. Spectrosc. **106**, 72 (1984).
[22] K. K. Irikura, R. D. Johnson, and J. W. Hudgens, J. Phys. Chem. **96**, 4306 (1992).
[23] H. Bock, B. Solouki, and G. Maier, Angew. Chem. Intern. Ed. Engl. **24**, 205 (1985).
[24] G. Jonkers, S. M. van der Kerk, and C. A. de Lange, Chem. Phys. **70**, 69 (1982).
[25] F. Melen and I. Dubois, J. Mol. Spectrosc. **124**, 476 (1987).
[26] H. van Lonkhuyzen and C. A. de Lange, Chem. Phys. **89**, 313 (1984).
[27] B. L. Kickel, E. R. Fisher, and P. B. Armentrout, J. Phys. Chem. **97**, 10198 (1993).
[28] J. H. D. Eland, *Photoelectron Spectroscopy*, 2nd ed. (Butterworths, London, 1984).
[29] R. D. Hudson and V. L. Carter, J. Opt. Soc. Am. **58**, 227 (1968).
[30] I. G. Simm, C. J. Danby, J. H. D. Eland, and P. I. Mansell, J. Chem. Soc. Faraday Trans. 2 **72**, 426 (1976).

[31] I. Powis, Mol. Phys. **39**, 311 (1980).
[32] B. Brehm, R. Frey, A. Kustler, and J. H. D. Eland, Int. J. Mass Spectrom. Ion Phys. **13**, 251 (1974).
[33] A. J. Yencha, A. Hopkirk, A. Hiraya, G. Dujardin, A. Kvaran, L. Hellner, M. J. Besnard-Ramage, R. J. Donovan, J. G. Goode, R. R. J. Maier, G. C. King, and S. Spyrou, J. Electron Spectrosc. Relat. Phenom. (in press).
[34] S. M. Mason and R. P. Tuckett, Mol. Phys. **60**, 761 (1987).
[35] M. S. Gordon and J. W. Caldwell, J. Chem. Phys. **70**, 5503 (1979). H. U. Lee and R. Janoschek, Chem. Phys. **39**, 271 (1979).
[36] J. F. M. Aarts and J. H. Callomon, Mol. Phys. **81**, 1383 (1994).
[37] T. A. Carlson, A. Fahlman, W. A. Svensson, M. O. Krause, T. A. Whitley, F. A. Grimm, M. N. Piancastelli, and J. W. Taylor, J. Chem. Phys. **81**, 3828 (1984).
[38] J. E. Hesser and K. Dressler, J. Chem. Phys. **47**, 3443 (1967).
[39] S. M. Mason and R. P. Tuckett, Mol. Phys. **60**, 771 (1987).
[40] I. R. Lambert, S. M. Mason, R. P. Tuckett, and A. Hopkirk, J. Chem. Phys. **89**, 2683 (1988).
[41] D. H. Mordaunt, I. R. Lambert, G. P. Morley, M. N. R. Ashfold, R. N. Dixon, C. M. Western, L. Schnieder, and K. H. Welge, J. Chem. Phys. **98**, 2054 (1993).
[42] G. Hagenow, K. Hottmann, and H. Baumgartel, Chem. Phys. Lett. **164**, 395 (1989).
[43] B. W. Yates, K. H. Tan, G. M. Bancroft, L. L. Coatsworth, and J. S. Tse, J. Chem. Phys. **83**, 4906 (1985).
[44] M. Suto, X. Wang, L. C. Lee, and T. J. Chuang, J. Chem. Phys. **86**, 1152 (1987).
[45] J. F. M. Aarts, Chem. Phys. **101**, 105 (1986).
[46] I. R. Lambert, S. M. Mason, R. P. Tuckett, and A. Hopkirk, J. Chem. Phys. **89**, 2675 (1988).
[47] *Eight Peak Index of Mass Spectra* (HMSO, London, 1970).
[48] J. F. M. Aarts (unpublished results).
[49] J. F. M. Aarts, Chem. Phys. Lett. **114**, 114 (1985).
[50] R. N. Dixon and R. P. Tuckett, Chem. Phys. Lett. **140**, 553 (1987).
[51] R. A. Bearda, H. R. R. Wiersinga, J. F. M. Aarts, and J. J. C. Mulder, Chem. Phys. **137**, 157 (1989).